Spot Ignition of Natural Fuels by Hot Metal Particles

by

James Linwood Urban

A dissertation submitted in partial satisfaction of the

requirements for the degree of

Doctor of Philosophy

in

Engineering - Mechanical Engineering

in the

Graduate Division

of the

University of California, Berkeley

Committee in charge:

Professor Carlos Fernandez-Pello, Chair
Professor Jyh-Yuan Chen
Professor Per-Olof Persson

Summer 2017

Spot Ignition of Natural Fuels by Hot Metal Particles

Abstract

Spot Ignition of Natural Fuels by Hot Metal Particles

by

James Linwood Urban

Doctor of Philosophy in Engineering - Mechanical Engineering

University of California, Berkeley

Professor Carlos Fernandez-Pello, Chair

The spot ignition of combustible material by hot metal particles is an important pathway by which wildland and urban spot fires and smolders are started. Upon impact with a fuel, such as dry grass, duff, or saw dust, these particles can initiate spot fires by direct flaming or smoldering which can transition to a flame. These particles can be produced by processes such as welding, powerline interactions, fragments from bullet impacts, abrasive cutting, and pyrotechnics. There is little published work that addresses the ignition capabilities of hot metal particles landing on natural fuels. The work presented here investigates the ignition capabilities of these particles by breaking the overall spot ignition process into three distinct subprocesses: generation, simultaneous transport and thermo-chemical change of the particle, and ignition of a fuel. This dissertation will present research on these subprocesses.

The first subprocess, generation, was studied through literature searches and the results are shown in Section 1.3 of Chapter 1 along with background on spot fires and previous and associated literature. Then in Chapter 2 a model for the heterogeneous oxidation of iron and steel particles is presented. In Chapter 3 results are presented on the ability of hot metal particles composed of four different metals to ignite a cellulose powder fuel. Then in Chapter 4, the ability of aluminum particles to ignite 6 natural fuels of different compositions and morphologies was investigated. Then the ability of aluminum and stainless steel particles to ignite a smolder in a grass powder fuel was investigated through experiments and modelling in Chapter 5.

Spot Fire Ignition; Wildland Fires; Biomass Combustion; Smoldering Ignition; Wildland Urban Interface Fires

To my family, friends, and all those in pursuit of things in this universe that can be known.

Contents

List of Figures

List of Tables

Acknowledgments

I would like to thank my family for supporting me, especially my mother and father. Their support, patience, and guidance has allowed me to be successful even when things seemed impossible. I don't think I give her enough credit, but my mom is largely responsible for what little of a work ethic I have. I remember hearing her say "It isn't easy until it's done", which at times was hard to hear, but this mantra has helped me get through the less glamorous parts of my graduate career such as writing chapters of my thesis so that I can enjoy the parts that are more fun. She has also been there, pushing me to be better not just when I need to, but because I can. I also must thank my father who has been an excellent role model as a PhD in Mechanical Engineering. From an early age my father made a point of talking to me about science and what he did as a scientist and why it was important. I don't think he did this to convince me to be a scientist, but it definitely ignited a scientific curiosity in me that still burns brightly. I also want to thank my brother Daniel, who has been an inspiration of helpfulness and kindness that I sometimes lack in comparison.

I would also like to thank Courtney who has provided so much love and support, especially during some of the toughest parts of a PhD program (Qualifying Exams, dissertation writing, conference deadlines, etc.), but also during fun times like camping trips, normal trips and climbing up walls in the rock gym. I'm excited to be provide the same love and support you and I'm excited for some future adventures.

Throughout my graduate education Prof. Carlos Fernandez-Pello has taught me so much and we've learned so much together through research. Carlos has been an amazing mentor - he is supportive, fun, and has pushed me to make sure the research I do is high quality and useful. A lot of the opportunities I've had to travel have been because of Carlos and for that I am also grateful. I have been incredibly luck to have him as an advisor and could not have asked for anyone better.

At Berkeley the graduate students in Hesse Hall have been great friends, peers, teachers, mentors, students, and fellow travelers. In particular, I am indebted to my friend and partner-in-science Casey Zak. In addition to being a great researcher to work with, his willingness to engage and dive deep into topics such as data presentation and experimental methods has made me a better researcher. Casey also is responsible for developing the experimental set up used in the experiments as well as the experimental techniques which I used to collect the data presented here.

Another person deserving special thanks is Sarah Scott. Sarah designed and fabricated the wind tunnel and sample holder used for the experiments presented here and later served as my mentor during my internship at Sandia, were I had the opportunity to learn about research at a national laboratory. It was incredible opportunity and I learned so much during my time there.

I would also like to thank Daniel Murphy who has served as amazing lab mentor. Dan constantly challenged me to find ways to do improvements on my research that I initially said were "too difficult" or "not practical". I would also like to thank others from Hesse Hall: Daniel Pineda, Maria Thomsen, Charles Scudiere, Xian Shi, Shmuel Link, Xinyan Huang, Andres Osorio, Danielle Kirchmeyer, and Jennifer Jones.

I would also like to thank the National Defense Science and Engineering Graduate Fellowship which as funded me for the last three years, it has allowed me to learn so much and I am so grateful.

Chapter 1

Introduction

1.1 Background

Fires can be started when hot small objects land in (or on) a fuel such as vegetation (e.g. dry grass, duff, litter, etc.), low density insulation materials, liquid or even gaseous hydrocarbon fuel. These hot small objects can be hot metal particles produced from hotwork, seized railroads brakes, transmission lines, and other sources, or from hot charring organic material, embers, also known as firebrands (for the purposes of this paper no distinction is made between the terms firebrand and ember) produced from burning material. The process by which these hot metal particles ignite a solid fuel is called spot ignition. This process is related to 'ember spotting', a process by which hot, burning, smoldering, or glowing combustible debris from a fire are lofted by the fires plume and then fall on and ignite fresh fuel. Ember spotting allows fires to rapidly spread by spot ignitions. There are sources in the literature which have compiled lists of spot fires and fires that have spread rapidly through ember spotting [5–10], however there are many spot fires which remain unreferenced.

Based on published data [6, 11], power lines, equipment, and railroads cause approximately 28,000 natural fuel fires annually in the United States. Some of these fires were catastrophic with extensive damage to land, property, and lives. In particular, fires caused by clashing conductors have the potential to grow more quickly than other fires because the conductor clashing is typically caused by high winds which also causes the fire to spread faster [12], thus the conditions where spot fires form clashing conductors occur are also conducive to fire spread. As an example, the Witch Creek and Guejito fires burned almost 200,000 acres and destroyed over 1,100 homes during the 2007 California firestorm. According to reports by The California Department of Forestry and Fire Protection (CalFire) and NIST, both fires were allegedly ignited by hot metal particles generated by power lines interactions [13, 14]. Another recent large wildland/urban interface fire is the Bastrop County Complex fire in Texas; the fire burned over 12,000 hectares in 2011 [8]. The fire allegedly started when power lines interacted with each other and nearby trees during high winds. The sparks produced by the powerline interactions fell on and ignited dried vegetation [8]. A more recent spot fire is the 2012 Taylor Bridge fire in the state of Washington; the fire was reportedly caused by

spot ignitions from rebar cutting and welding sparks from construction of an underpass fell on and ignited dry vegetation [15]. The fire eventually consumed in excess of 23,000 acres and destroyed approximately 60 homes and in excess of 200 outbuildings [15]. Spot fires have also occurred in other countries. In New Zealand 275 fires were ignited by embers, sparks, or flying brands between 2005 and 2010 [7]. In Australia, some of the wild fires of the Black Saturday event of February 2009 were also allegedly generated by sparks and propagated extremely fast by ember spotting [16]. Particles and sparks produced by welding, grinding and various forms of hot work have also been involved in several other notable incidents, and the established literature discusses many potential hot particle sources [1, 2, 5, 9, 17–21].

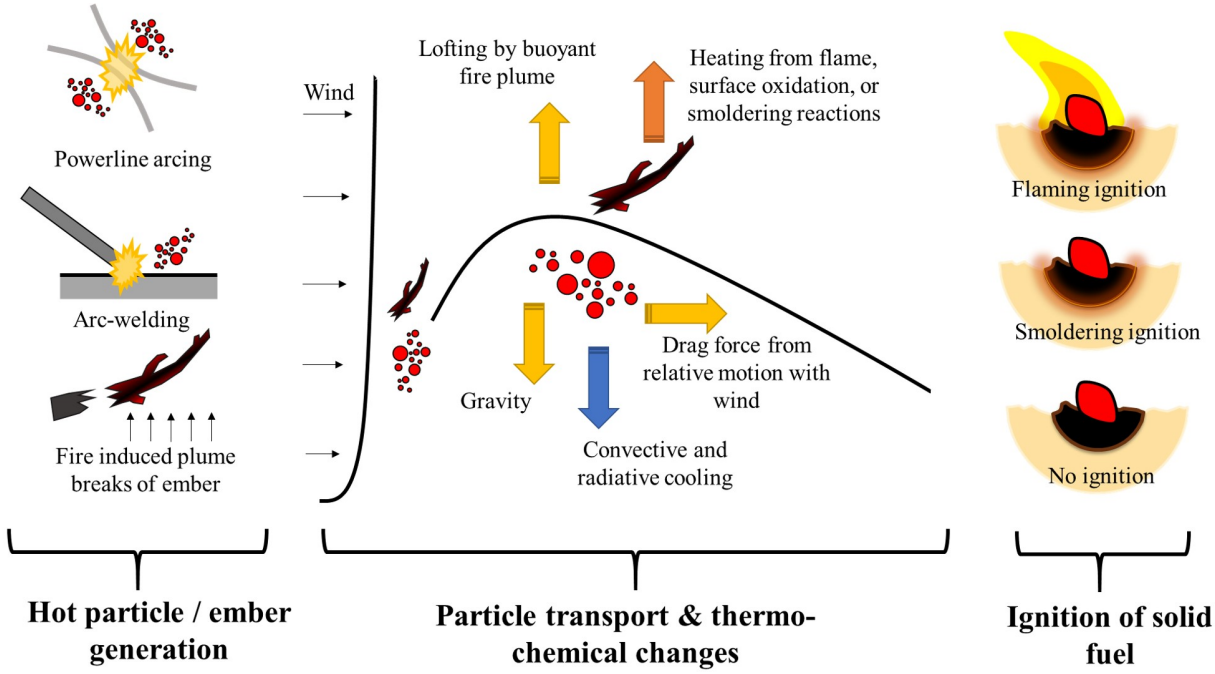

Figure 1.1: Spot Ignition Sub-processes: particle generation, coupled transport and heating/cooling, and possible ignition upon contact with a fuel

1.2 Spot Fire Ignition Processes

The spot fire ignition problem can be separated into several individual processes which are shown in Figure 1.1. The first section depicts methods by which hot metal particles and ember can be produced. It should be noted that there are of course other sources of hot metal particles such as bullet fragments after impact [19] and pyrotechnic debris [21] to name a few. The second section shows the processes which can occur as the particle falls. The third section shows the potential for flaming and smoldering ignition to occur. Then if ignition occurred, the subsequent flame/smolder spread

processes (independent of the particle) and the possible transition from smoldering to flaming can occur. Determining the precise moment when 'ignition' occurs - especially in a spot ignition situation can be difficult. For the purposes of the research presented here we will consider 'spot ignition' to be when the combustion reaction front is independent of the ignition source. In the followings sections of this chapter will provide an overview of the mechanisms by which hot particles are generated (Sec. 1.3), transported (Sec. 1.4), heated or cooled by thermo-chemical changes (Sec. 1.5), and finally the ability of these particles to ignite a fuel (Sec. 1.6). And in later chapters I will discuss the coupled transport and thermo-chemical change (Chapter 2 and subsequent spot ignition (Chapters 3,4, & 5).

1.3 Generation of hot metal particles and embers

The generation of hot metal particles typically requires a source of energy and enough impulse to expel the hot particles from the source. There are many combinations of heat sources and ejection processes as there are particle generation processes. Some common generation processes are described below.

Arc Welding

Arc welding can be largely broken down into three main methods which are commonly used. Gas Metal Arc Welding (GMAW) also known as Metal Inert Gas (MIG) welding, Shielded Metal Arc Welding (SMAW) also known as 'stick' welding, and finally Tungsten Inert Gas (TIG) welding. In both GMAW and SMAW, the electrode is consumed while in TIG welding it is not. Both GMAW and TIG use an inert gas (e.g. carbon dioxide or argon) to displace oxygen. SMAW uses a material commonly called 'flux' which will vaporize during arcing, displacing oxygen. The partially degraded flux can condense on the weld as 'slag'.

The process of arc welding requires locally heating and melting a metal. If overheating of the molten metal occurs it can cause local vaporizations of the metal, ejecting particles outward. Also, SMAW can cause a large welding bead to form on the tip of the stick. If the stick is discarded by the welder before the bead has cooled, a human could server as the "ejection process". For welding spatter, temperatures near the arcing have been measured from 1850 °C and particle sizes ranging from 0.1 mm [22] [22] to 3mm [23] and in rare cases ($< 0.1\%$) particles as large as 6-7 mm in diameter [23]. A recent study found that the number of particles produced by SMAW increased with increased current and the size of the spatter particles increased with decreased voltage [24].

One study [25] found that Gas Metal Arc Welding (GMAW) could produce single droplets of molten steel with sizes up to 3.75 mm in diameter. The particle diameter appeared to have a negative correlation with wire feed rate. This research also showed that larger wires (1.2 mm vs. 0.9 mm) tended to produce larger particle diameters [25]. In the same study, measurements of the velocity of the welding droplets was performed. The experiments showed that increasing the electrical current, I, would increase the velocity of the particles [25]. The authors then performed

a simple energy balance equation, Eqn. 1.1, between the droplet speed and the work done by the electromagnetic force.

$$\frac{\pi}{6}\rho d_p^3 v_p^2 = \frac{I^2 \mu_0}{4\pi} d_p \Psi \tag{1.1}$$

where v_p is the ejection speed of the particle, I is the current, d_p is the size of the particle, μ_0 is the permeability of free space, and $\Psi = \int f(s)\frac{ds}{d_p}$ is a non-dimensionalized shape factor assume to be near unity. From this force balance they derived an equation of the form ($v_p = c \cdot I/d_p$) but were unable to fit their data do the calculated constant, c due to an error in the derivation, so instead they presented only an empirical fit. After correcting the algebra error I attained Eqn. 1.2 which produces a constant that matches the experimental data.

$$v_p = \frac{I}{d_p}\frac{1}{\pi}\sqrt{\frac{3\mu_0\Psi}{\rho_p}} \tag{1.2}$$

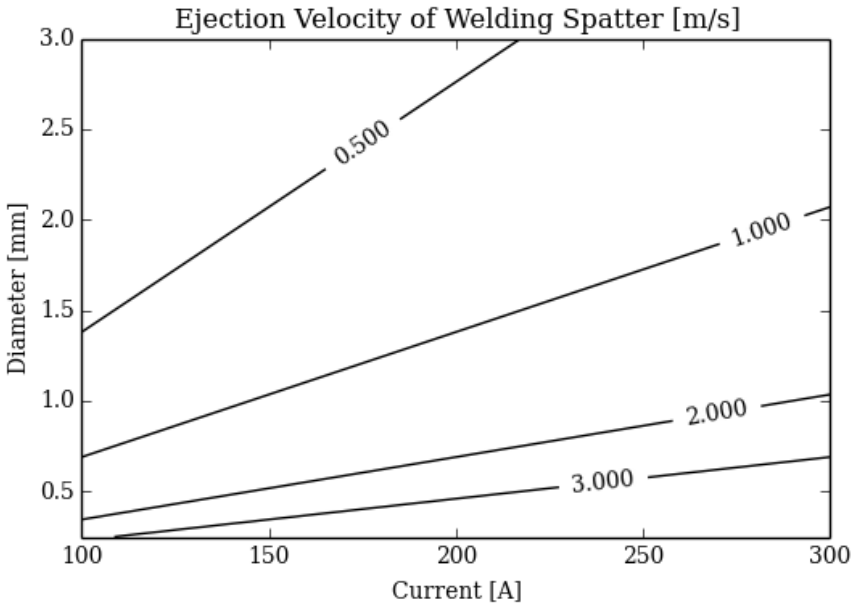

Figure 1.2: Ejection Speed of Welding Droplets from GMAW using Eqn. 1.2

The results of this equation are shown as a contour plot in Fig. 1.2. We see that for the particle sizes shown the speed is on the order of 1 m/s, and agrees with the experimental velocity measurements obtained by [25].

Bullets and Ammunition

Hot metal particles can be created by impacts of bullets with rocks. A study by the US Forest Service found showed that the deformation that occurs when a bullet hits a hard object can cause heating and ignite a fuel [19]. There have also been reports of tracer rounds (special bullets that are designed to oxidize with the surrounding air and subsequently glow due to their heat so they are visible to the shooter) [26].

Conductor Clashing

In the case of hot aluminum particles created by arcing power-lines, the electrical contact between the two conductors causes high electrical currents to flow through the point of contact which heats the wire locally. If the heating is strong enough it can locally vaporize the metal and eject the metal with the force from the expanding metal vapor [27]. If the heating is not as strong, the metal could be ejected due to the wind and/or motion of the wires from the arc or the high winds.

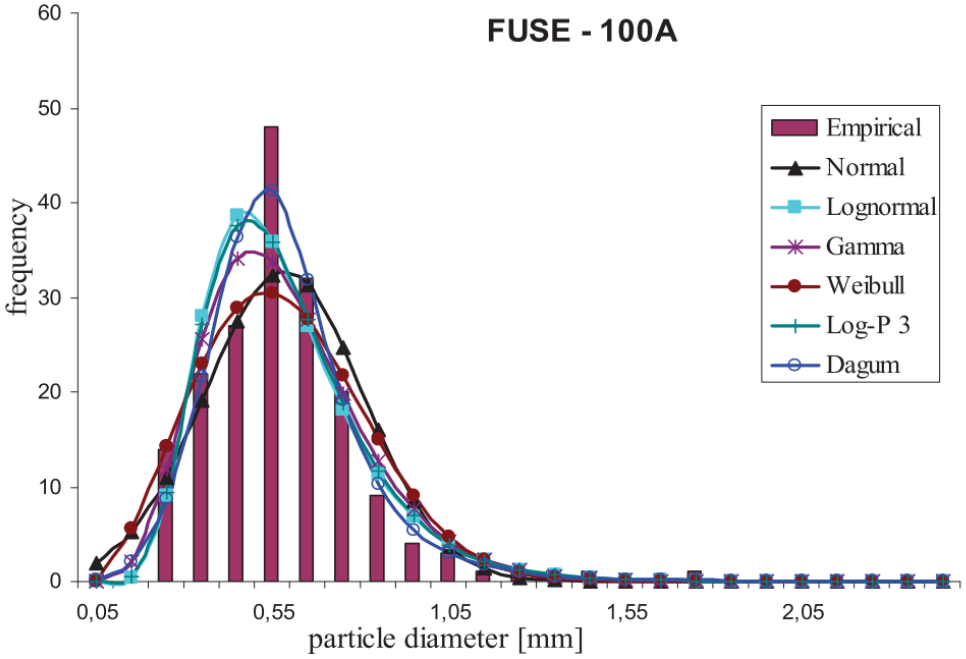

Figure 1.3: Size distribution of aluminum particles created by discharge with a fuse of 100 A from [1]

There has not been any reported measurements of aluminum particle temperatures, but there have been measurements of the particle size distribution by researchers [1] shown in Fig 1.3. We can see that the particle sizes are typically below 1mm with some particles being larger than 1 and even 2 mm.

Embers and Firebrands

Manzello et al. did several experiments characterizing the firebrands produced by single trees burning and measured the size and mass distribution of these embers [28–30]. Then Manzello and others at NIST developed a device named the "Dragon" to create and eject embers [31] with the size and mass distribution of the embers comparable to those produced from the single tree burn experiments [28–30]. In addition to providing a way to create firebrands quickly in an experimental setting, the Dragon also allowed for testing of fire brand sprays instead of small batches of firebrand ignition experiments [29, 32–34]. Later the Dragon was augmented with the "Dragon's LAIR (Lofting And Ignition Research)" which allowed for the firebrands to be lofted and pushed by a simulated crosswind [35]. While the Dragon devices are not the natural way firebrands are produced, they have become the standard method for making an ember shower in a laboratory setting.

If drag forces from the airflow around a piece of burning material is strong enough break it off from the test of material embers [36]. This is made easier because the thermal degradation from fire exposure weakens the strength of the material making breakage easier. Tohidi used a simple breakage model in a Monte Carlo simulation [36] to explain the size and mass distribution of embers measured in experiments by Manzello [28–30]. Embers can also be caused by interactions of vegetation with powerlines [37], where ohmic heating causes the tree to heat and smolder or flame [37].

1.4 Transport of hot particles and embers

After a hot particle or ember is generated and ejected it will experience the force of gravity, drag forces from the relative motion of the gas (ambient air or hot smoke plume from a fire) around it. At the same time, the particle will be exchanging heat with the environment by radiation and convection heat transfer and if the conditions are right, chemical reactions may heat the particle simultaneously which is discussed in the next section.

Forces During Particle/Ember Transport

As a particle or ember falls it will experience aerodynamic drag forces and gravity. The drag force will be aligned with the direction of the relative motion of the gas around the particle. Thus depending on the situation the wind can either slow the particle or accelerate it. A diagram showing the basic equations of motion and free body diagram is shown in Fig. 1.4.

Sparks from power-lines

Power and data transmission lines are commonly made of aluminum, copper and in some cases steel for structural support. The material of the particles greatly effects the thermo-chemical processes the particle undergoes and in some cases heavily influence the trajectory of the particle. A paper by Tse and Fernandez-Pello showed that aluminum sparks could burn in the gas phase as

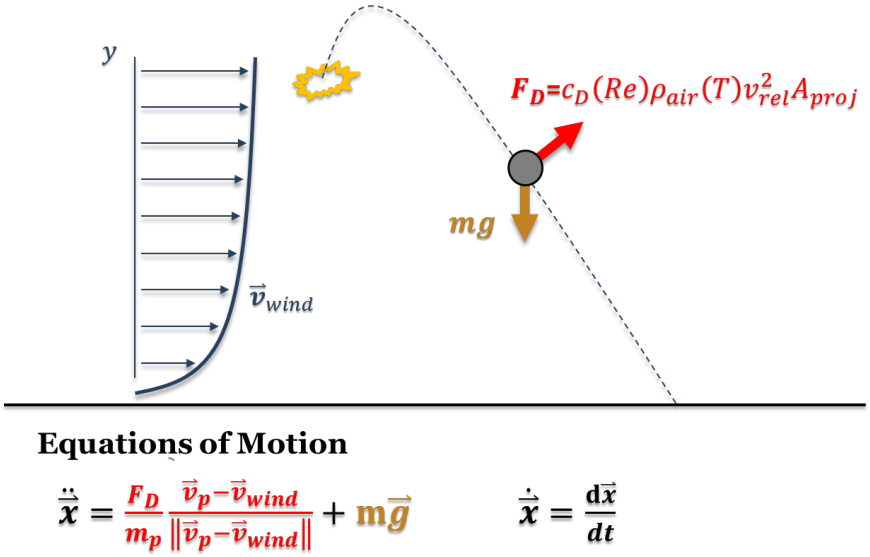

Figure 1.4: Forces that effect particle motion

they fell [38]. This in turn would cause the particle to shrink as it fell, increasing its surface to volume ratio and thus if backed by a strong wind, the spark could travel substantially farther. This study also showed that if the fall was long enough the spark could be consumed to the point that it would be too small to pose any significant ignition hazard. Tse and Pello also considered copper particles from conductor arcing and simulated them as they fell [38].

Hot work (welding, abrasive cutting, and flame cutting)

The work by Mikkelsen [2], examined the temperatures, sizes, and travel distances of particles produced by various hot work operations by measuring tool and workpiece temperatures and using burn paper to see the size and landing locations of particles. The final landing distances (maximum and average) are displayed in Table 1.1. Examining the results for GTAW and SMAW we can see that on average the metal particles do not travel that far, however some particles are able to travel significant distances (up to 7.5 m) without the aid of a cross wind and minimal dropping distance and thus travel time. The National Fire Protection Association (NFPA) has published guidelines for the use of welding and other hot work equipment[5].

In particular the NFPA recommends roughly 11 meters (35 feet) between the hotwork and potential fuels [5]. This separation distance is validated by the results of Mikkelsen [2]. However the safe separation distance would need to be greater in situations where the welding spatter would fall a longer fall distance and/or significant wind. However as seen in Mikkelsen's results, the average distance traveled is quite low. It is possible that welders might ignore the 35 foot distance if they see that the average particles only travel 1m and do not anticipate the errant particle that travels to the maximum distance. Mikkelsen also recorded long exposure photographs of the trajectories

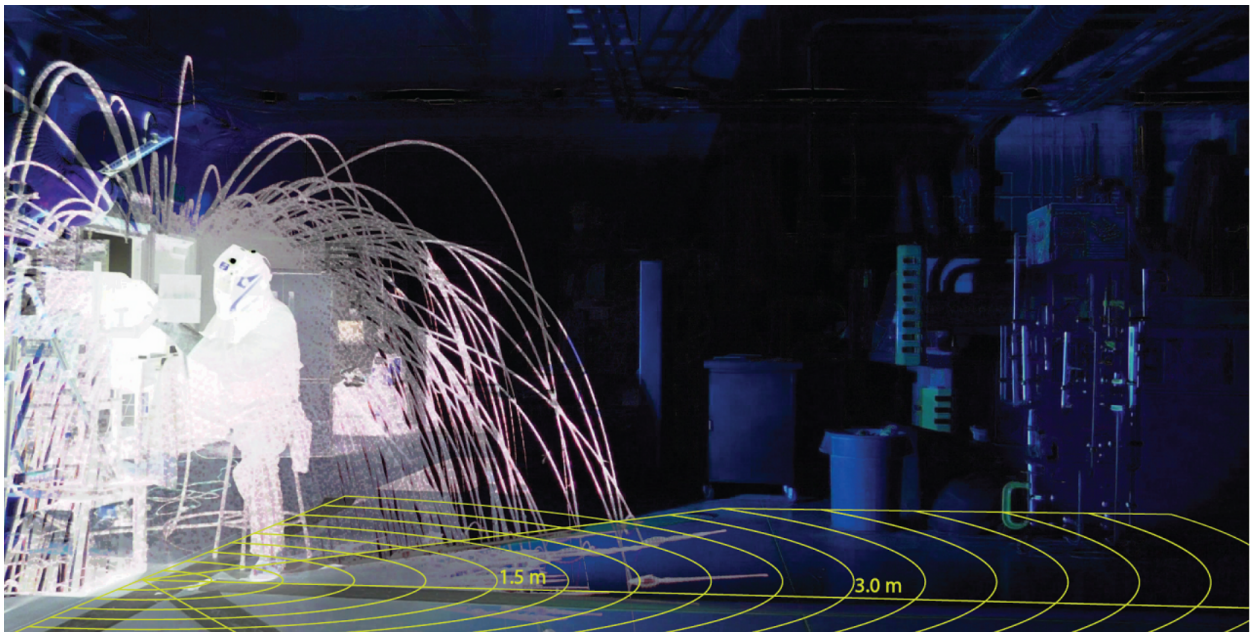

Figure 1.5: Particles ejected by Gas metal arc welding (long camera exposure) from [2]

of the welding particles were taken. One such photograph showing the ejection of these particles is shown in Fig. 1.5. We see that the particles travel up to 2 m away without the wind.

For hot metal particles, gas phase combustion is possible if the Glassman criteria is satisfied [39], such is the case with burning aluminum particles. The flame will boil the outer surface of the molten particle and deplete the aluminum [38]. Alternatively surface oxidation of the bare metal can heat the metal particles and increase their temperature. The oxide layer formed by oxidation can prevent the reaction of the metal with oxygen in the air in that case the hot particles will then simply cool as they fall.

There are several studies on in the transportation and thermo-chemical processes that occur during the flight of hot metal particles. Several have examined the flight of metal particles from aluminum power-lines [27, 38, 40] and inert particles falling from copper power-lines [38]. There have also been studies on embers falling through ambient air [38] as well as embers in a fire's plume[41]. Recently a paper on inert debris from pyrotechnics was modeled by [21]. Chapter 2 will present work by the author on the ways in which oxidation reactions heat metal particles as they fall.

Table 1.1: Landing locations of particles generated from hotwork from [2]

Process	Case	$D_{MAX}[m]$	$D[m]$
GTAW - SMAW	Nominal 1	3	0.5
GTAW - SMAW	Nominal 2	6.5	0.5
SMAW	Worst 1	4.8	0.6
SMAW	Worst 2	7.5	0.6
GMAW	Nominal	3.3	0.6
GMAW	Worst	4	0.6
Arc Gouging	Nominal 1	9.4	1.1
Arc Gouging	Worst 1	9.9	1.1
Arc Gouging	Worst 2	8.3	1.8
Arc Gouging	Worst 3	8	1.4
Plasma Cutting	Nominal 1	6.8	1.4
Plasma Cutting	Worst 1	7.3	1.4
Plasma Cutting	Nominal 2	7.9	1.9
Plasma Cutting	Worst 2	6.4	1.9
Plasma Cutting	Nominal 3	5.7	1.6
Plasma Cutting	Worst 3	4.6	1.1
Plasma Cutting	Nominal 4	8.4	1.3
Plasma Cutting	Worst 4	5.8	1.1
Oxyacetylene Cutting	Nominal	4.7	1.1
Chop Saw Guard In	Nominal	7.9	1.1
Chop Saw Guard Out	Worst 1	7.1	2.6
Chop Saw No Guard	Worst 2	8.8	4.1
Cut Off Wheel	Nominal	5.6	2.1

1.5 Thermo-chemical change of Hot Particles and Embers During Transport

As hot metal particles are transported 1.4, they can undergo thermo-chemical changes which can change many aspects of the particle. As such the transport and thermo-chemical change processes often cannot truly be decoupled as they are happening simultaneously. However, in some cases it might possible to ignore or simplify some of the processes. To characterize this we can consider a given particle or ember traveling with a heat transfer time, t_{HT}, which is the characteristic time for the particle to come arbitrarily near to thermal equilibrium with the surroundings (through convection and radiation) as it falls. Then we can consider the mass transfer time t_{MT} of the particle which is the time it takes for any phase change or chemical reactions to come arbitrarily near to completion. If we non-dimenionsalize these times by the motion time of the particle, t_{motion}, we get an indication of how far these processes would progress before the particle lands. The different regions are shown in Fig. 1.5.

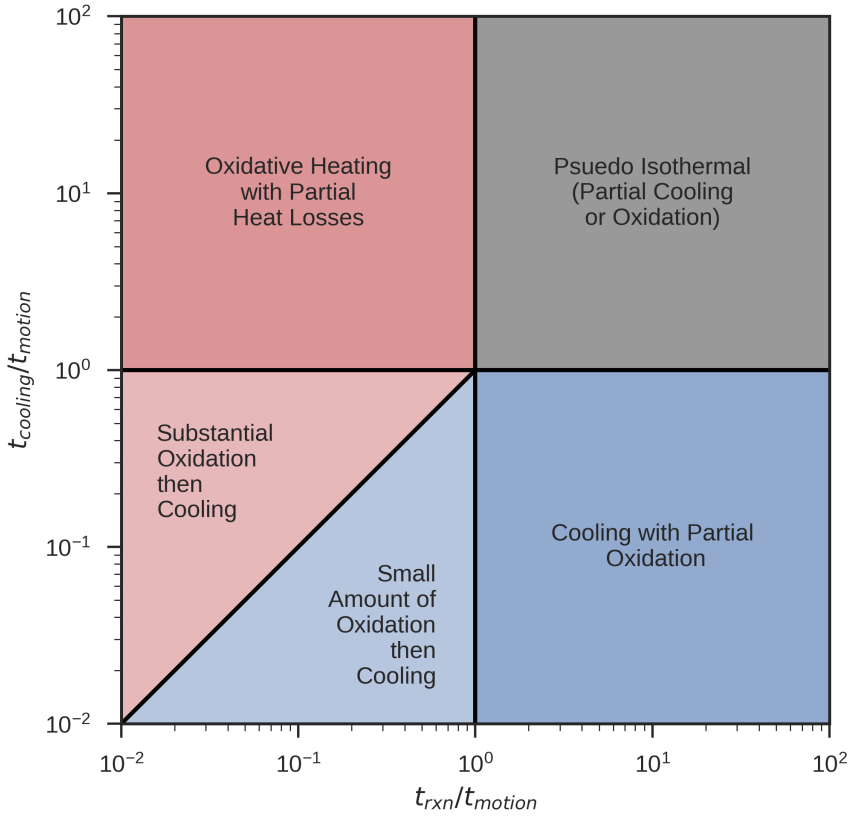

Figure 1.6: Comparison of hot particle transport and thermo-chemical change regimes based on timescales (log-log scale)

The labeled regions of the graph are colored according to the net heating or cooling that the particle is likely to experience (and not necessarily the final temperature or danger posed by the hot particle). This figure is useful for showing change in the ignition hazard posed by the particle after it is generated, but it is not a quantitative measure of ultimate ignition hazard. This graph is instead intended to examine how the combined heat transfer and mass transfer processes change the relative ignition danger which can be a little counter-intuitive to some. One is example of this is that shortening the time required for the particle to react does not necessarily increase the ignition hazard. If we examine the region labeled ”Substantial Reaction then Cooling” we see that because the reaction will happen so quickly the particle will also have time to cool as it falls so it may pose less of an ignition hazard despite possible experiencing substantial heating during its trajectory.

Gas Phase Combustion of Metals

The ability for a metal to burn in the vapor phase is dictated by the Glassman criterion, which states that the volatilization/dissociation temperature of the oxide must be higher than the boiling

point of the metal for vapor phase metal combustion to occur [39] and of course the metal exposed to the oxidizer be raised to its boiling point.

If a flame is ignited it will envelope the droplet or if the Reynolds number is too high, $Re > 138$, the flame will anchor in the wake region behind the particle [38]. For an enveloped flame, the droplet will then evaporate at its surface depleting the metal according to the d-squared law shown in Eqn. 1.3.

$$d^2(t) - d_o^2 = K(t - t_o) \tag{1.3}$$

where K is the burning rate given by Eqn. 1.4 from [42].

$$K = K^0(1 + 0.276Re^{1/2}Pr^{1/3}) \tag{1.4}$$

During this process the temperature of molten metal will be the boiling point of the metal.

Surface Oxidation of Iron and Steel

If the conditions are right, metal particles can experience surface oxidation reactions. As the oxide layer forms it will make it increasingly difficult for oxygen to reach the unreacted metal, and thus diffusion of oxygen across the oxide becomes important. However when some metals oxidize the oxide layer will crack because the newly formed oxide has a lower volume per molecule of metal. There is a parameter which characterizes this behavior, the Pilling-Bedworth Ratio, z. If $z < 1$, then cracks will form and if $z > 1$ then a protective layer is formed. Eqn. 1.5 gives the Pilling-Bedworth Ratio.

$$z = \frac{\rho_{Me} M_{MeO_\gamma}}{\rho_{MeO_\gamma} M_{Me}} \tag{1.5}$$

When the cracking forms the oxidation is more chaotic and not as well characterized while when the protective oxide is formed the oxidation process is better characterized. However before diffusion across the oxide layer is important the oxidation process is first governed by the convective transport of oxygen to the surface of the metal and is discussed later Chapter 2. Some prior studies [43, 44] have ignored this effect and as such their models predict unphysical heating of the metal sparks.

Another criteria for metal oxidation to occur is for the metal be at a sufficiently high temperature. Below 700°C, oxidation is chaotic and minimal. As such, low temperature sparks such as those considered in [45] exhibit minimal oxidation and pose little threat.

Combustion of Embers and Firebrands

Firebrands and embers can burn with a flame or through glowing combustion as they fall. The gas phase combustion processes have been modeled by Tse [38] and Anthenien [41] and others. As the reaction progresses the ember will typically char until it is only char at which point flaming combustion will not be sustained it will revert to glowing or cooling. The gas phase combustion can be hindered if the ember is in the plume from a fire where oxygen concentrations are low [41].

1.6 Ignition of fuels of hot metal particles and embers

The ignition of a fuel bed by a hot metal particle is very complex. Once the hot particle lands on the fuel bed its energy is transferred to the fuel and ambient surroundings. If the particle has enough energy the fuel near the particle is heated and may pyrolyze. This process in turn cools down the particle. The pyrolyzate mixes with the air and a flammable gaseous mixture may be generated near the particle. If the particle is still hot enough it can act as a pilot and ignite the gaseous mixture. If it is not hot enough to act as a pilot the particle can still provide enough energy to initiate the ignition of the gas by an auto-ignition process. Alternatively, the hot metal particle can initiate a self-sustained smolder in the fuel bed that may eventually transition into a flame. This complex ignition process depends on several factors, including the size and state of the metal particle (temperature, molten, or oxidizing), the characteristics of the fuel bed on which it lands (temperature, chemical composition, geometry, density, or moisture content), the dynamics of the particle landing (fully or partially embedded on the fuel bed, bouncing, or splashing) and environmental conditions (temperature, humidity, or wind velocity). Obviously, the study of such a complex phenomenon must be parameterized.

There are a growing number of studies published on the ignition of fuels by hot metal particles [3, 46–57].

Ignition of Natural and other Ligno-cellulosic Fuels by Hot Metal Particles

Tanaka, [48], studied the ignition of sawdust by welding spatter at various fuel moisture contents. Then Stokes [47] studied the ability of metal particles produced by arcing wires to ignite various fuels. Later Rowntree and Stokes conducted a study controlling both size and temperature and examined the ability of hot aluminum particles to ignite barley grass [3]. Hadden et al. [46], conducted work studying the potential of stainless steel particles to smolder or flaming ignite powdered cellulose beds. Other researchers have also studied various other aspects of this problem. [51] studied ignition of powdered cellulose by contact with stainless steel and brass particles while also varying the moisture content of the cellulose fuel beds. Then Zak et al. developed a statistical treatment of similar data with steel particles falling onto cellulose fuel beds [52].

Urban et al. studied the effect of different metal particle types (aluminum, brass, copper, and steel) igniting powdered cellulose fuel bed with a flame [49] which Zak modelled with a simplified 1-D ignition model [54]. This model was compared to experiments presented in Chapter 3. Then Urban et al. did a study [57] examining at the ability of hot aluminum particles and droplets to ignite α-cellulose (as a powder and paper strips), pine needles (as needles and as a powder), and a grass blend (as blades of grass and as a powder) and discussed further in Chapter 4. Urban et al. also examined the process by which steel and aluminum particles ignite a smolder in a grass blend powder [50] and used a simple ignition model to show that for smoldering ignition the particle can act as a heat sink, hindering the smoldering front. Recently Wang et al [55] studied the ignition (smoldering and flaming) of pine needles of various moisture contents by hot large stainless steel particles and smoldering to flaming transition.

Ignition of Plastic Polymers by hot Metal Particles

There have been several studies on investigating the ability of hot metal particles to ignite plastics on fire. Investigators have simulated the ignition of Polyurethane foam by a hot metal particle by characterizing the material scale with Thermo-Gravimetric Analysis and Differential Thermal Calorimetry [58]. They later investigated ignition of low-density polystyrene foam through ignition experiments with hot metal particles. In their work they characterize this ignition process thoroughly and noted that the metal particle could tunnel through the foam significantly due to the high particle temperature melting the foam[59]. They also studied the ignition of an expanded polystyrene foam through experiments and numerical modeling [60]

Ignitions of Energetic Materials (Solid Propellants and Explosives)

Before the studies on the ignition of wildland fuels by hot metal particles, there was substantial research on the ability of hot metal particles to ignite energetic materials such as the propellant of solid rocket motors or stored explosives. A major motivation was to understand how to prevent a method of ”sympathetic detonation” where debris from an explosion ignites the solid propellant [61] of a solid fuel rocket motor.

Ignition by Embers and Firebrands Single embers and showers

Upon impingement with the ground, firebrands can be either burning with a flame, undergoing glowing combustion and/or smoldering, or they may be minimally reacting and just cooling. Manzello studied the ability of single firebrands in either a glowing and flaming state to ignite pine straw, hardwood mulch, and cut grass beds and found that it was possible but unlikely for glowing firebrands to ignite these fuels even when they were very dry [33]. However flaming firebrands were capable of igniting the finer fuels, but when the fuel had a FMC of 11%, ignition was not observed for the hardwood mulch and observed half of the time for the cut grass [33]. Another study specifically on the effect of fuel moisture content on the ignition time of pine needles exposed to an ember, the results show that the ignition time has a linear relationship with the square of the fuel moisture content [62]. There has also been numerical modeling of the ignition of alpha cellulose by an ember using FDS (Fire Dynamics Simulator)[63] and Gpyro[64, 65], a solid fuel pyrolysis solver[66]. Manzello et al. also studied the ability of firebrands to ignite parts of home such as ceramic roofing assemblies [67]

Another aspect effecting the ignition of fuels by embers is the fact that when significant amounts of embers in an ember storm accumulate, they will increase the ignition capability because the ”pile” of embers will act like a much larger one [56]. Manzello has examined how embers produced form the ”Dragon” ember generator can ignite mulch in ”re-entrant corners” like those found in homes which can then ignite the siding [68]. Manzello et al. also studied siding treatment and components to ember showers and investigated the vulnerabilities of the different components.

1.7 Goals of Present Work

The work presented in this thesis was undertaken with the goal of determining the process by which hot objects ignite natural fuels and to examine how some of these hot objects become hot. Chapter 2 will investigate the mechanism by which iron particles can oxidize, allowing them to self-heat and stay at higher temperatures longer. Then Chapter 3 will discuss experiments on the ignition of cellulose fuels by hot metal particles (steel, copper, aluminum and brass). Chapter 4 investigates the ability for aluminum particles to ignite different natural fuels (dry grass, pine litter and cellulose) in powder and larger pieces (blades of grass, pine needles, and paper strips). Then Chapter 5 investigates the ability of aluminum particles to ignite a smolder in a fuel bed made by grinding dry grass into a powder. These results combined with data on the information about hot particle generation in Section 1.3 provide information on the three subprocesses of the spot fire ignition process and provide a framework for simulating specific spot fire ignition scenarios (particles produced from other processes, different fuel and particle types, different particle reaction behavior as the particles fall).

Chapter 2

Oxidative Heating of Hot Metal Particles and Sparks

The coupled heat and mass transport occurring when a hot metal particle (spark) undergoes an oxidation surface reaction were numerically simulated under conditions consistent with those which could reproduced by welding, grinding, metal cutting and other hot work processes which produce these metal sparks. It was shown that for iron sparks, the initial stage of oxidation is primarily limited by the transport of oxygen to the sparks surface through the ambient air and then after the accumulation of a significant oxide layer, the oxidation becomes limited by the diffusion of oxygen across the oxide layer.

2.1 Introduction

Hot metal particles/sparks can ignite fires when they come into thermal contact with a solid fuel. These sparks initially become hot during metal cutting, grinding, welding, other hot-work processes or seized train brakes. This work will show that under certain conditions, these sparks will experience exothermic surface oxidation reactions which can increase the temperature of the sparks and offset heat losses to the environment, enhancing their potential to start a fire. For this to happen oxygen must be transported from the surrounding gas to the reaction front in the spark. This process involves the transport of oxygen through the boundary layer and then trough the oxide layer of the particle. Previous models of the spark oxidation have neglected the limiting effect of gas phase oxygen transport to the sparks surface. The added restriction of the gas phase oxygen transport allows the spark to ration the unreacted metals stored chemical energy. Thus, these sparks land at higher temperatures increasing the danger they pose. Although much of the discussion in this chapter will be independent of the actual metal of the spark, however Iron will be used as an ubiquitous example because of its presence as one of the most common usage in the hot work processes which create these sparks.

The mechanism by which metal sparks oxidize causing them to self-heat is complex and involves oxygen transport in the ambient gas to the sparks surface and oxygen transport across the

oxide layer [69, 70] and a solid phase chemical reaction. There are also constraints on the conditions over what temperature oxidation will occur. At temperatures below 570°C, substantial oxidation does not occur in part because the simplest oxide of iron, FeO, is not thermodynamically stable and oxidation experiments conducted below 570°C displayed inconsistent oxidation behavior, presumed to be caused by the sample preparation [70], instead smaller oxide layers of another iron oxide (Fe_3O_4) will form. Similarly, oxidation at temperatures between 570-700°C is minimal and experimental studies have found that the oxidation was heavily dependent on the sample preparation [70].

For temperatures above 700°C, the surface oxidation process is well characterized up to 1250°C and it has been shown that 95% of the oxide layer formed is FeO [70]. The combustion of iron in atmospheric air has been shown to occur as a solid phase oxidation reaction [71] while at high temperatures and pressure in elevated concentrations of oxygen gas phase combustion has been observed to occur in the gas phase [72]. The ability for a metal to burn in the vapor phase is controlled by the Glassman criterion, which states that the volatilization/dissociation temperature of the oxide must be higher than the boiling point of the metal [39] and of course the metal exposed to the oxidizer be raised to its boiling point. This work only simulates scenarios where the temperature of the metal is below its boiling point and the volatilization/dissociation temperature of its primary oxide and thus vapor phase metal combustion does not occur.

There is a common misconception that oxidation of small metal sparks (0.5 - 2 mm) is solely limited by oxygen diffusion across the oxide layer. As a result, much of the current literature of the oxidation of metal sparks ignores the limiting effect of gas phase oxygen supply to the sparks surface [43, 44]. This misconception is likely due to researchers applying oxidation models commonly used in metallurgy studies to the oxidation of metal sparks. The metallurgy studies typically examine longer term oxidation behavior of much larger samples where the gas phase oxygen delivery is not as important at the timescales they are considering. In these studies, the oxidation of the metal sample takes place over timescales of the order of 1000s [69] while in this study the oxidation of the sparks takes place over timescales of the order 1s. Furthermore, the sample sizes in the metallurgical studies are large enough such that the oxide layer is relatively thin compared to the sample while for the oxidizing sparks, most of the spark can be oxidized. There are however, a few studies in the metallurgy literature that examine the effect of gas phase oxygen transport on the rate at which metals oxidize [69, 73, 74] Spark oxidation and burning models like the present work and others [38] can be used in conjunction with studies such as those by the author [49, 50, 50–53, 56] which investigate the ability of these hot metal particles to ignite natural fuels with both a flame and or a smolder to enable assessment of the danger of various particle sources.

2.2 Model Description

In this study we have made several assumptions about the oxidation process of an initially pure metal suddenly exposed to an oxidizing atmosphere. The first assumption is that thermal transport inside the particle is infinitely fast.

Assumptions:

- Thermal transport inside the metal spark or hot particle is instantaneous
- Oxidation reactions are instantaneous
- The oxide layers of the various iron oxides can be considered to be one net oxide layer which has isotropic material properties
- Absorption of the oxygen at the surface of the particle is instantaneous and all oxygen can adhere to the surface
- The oxide layer does not have voids or porous gaps
- The oxidation process is 1-dimensional (radial in spherical coordinates).

Oxidation Model

Chemistry

When iron undergoes oxidation reactions the products are a combination of its three oxides: FeO, Fe_3O_4, and Fe_2O_3. The relevant chemical and material properties of the iron and its three oxides are given below in the table. In most cases only an outer surface of the iron is directly exposed to the oxidizing environment, in this case, air. For Wustite, FeO, the only oxide considered for this study, the relevant global chemical reaction is

$$Fe_{(s/l)} + \frac{1}{2}O_{2(g)} \rightarrow FeO_{(s/l)} + Q_{ox} \tag{2.1}$$

Build up of Oxide layers on spark surface

The oxides form in layers on the outer surface of the metal and then progresses inward. The oxide layer is divided into three distinct oxide layers, one for each oxide. The outermost layer exposed to the oxidizing environment is typically hematite Fe_2O_3, followed by magnetite Fe_3O_4, then wustite, FeO. In manufacturing and metallurgical literature, the process of this multi oxide layer forming is referred to as scaling and the composite layer is called 'scale'. Typically the relative scale size of the different scales are 1%, 4%, and 95% [75]. For the present study we have chosen to simply the analysis by assuming that the oxide layers is only composed of Wustite, FeO. We feel that this is reasonable as the wustite is 95% of the scale thickness according to [75]. As the oxide layer forms around on the outside surface of the spark the sparks mass increases from the addition of the oxygen. Simultaneously the overall size of the particle increases because the oxide layer is less dense than the pure metal.

Mass and Volume Change

Certain metals can form an oxide layer on their surface which will slow the transfer of oxygen. Their ability to do so requires two criteria: the heat released during the reaction does not heat the oxide or the metal to its boiling point and the Pilling-Bedworth Ratio, z, must be greater than unity. Eqn. 1.5 gives the Pilling-Bedworth Ratio which is the relative change in volume when you react one mole of mole of unreacted metal completely [76].

$$z = \frac{\rho_{Me}}{\rho_{MeO_\gamma}} \frac{M_{MeO_\gamma}}{\rho_{Me}} \tag{2.2}$$

For simplicity, z and the densities of the oxide and metal were assumed to be constant and independent of temperature. When $z < 1$, the oxide has a lower molar specific volume based on the number of the number of metal atoms and as metal atoms are oxidized the resulting oxide will contract and crack. This will in turn expose bare metal below making the oxidation faster and chaotic, thus more difficult to characterize. If $z \geq 1$, then the resulting oxide layer will not crack due to this contraction and thus will form a protective layer around the unreacted metal. Thus, in this study we will only examine the sparking ability of metals where $z \geq 1$.

The oxide layer formed on the surface of the metal will grow as the oxidation progresses. Because $z \geq 1$ the spark will swell and the overall size and mass of the spark will increase. To account for the increase in size as the spark reacts we can parameterize the change in volume and mass by the fraction of the original metal oxidized on a per mass or volume basis, X, in the same manner done in a prior study of the oxide layer growth in small nickel spheres [77]. The overall diameter of the particle, d_p, and of the unreacted metal core, d_{Me} can be written as a function of the initial diameter of the unreacted spark, $d_{p,o}$ and X as shown in Eqns. 2.3 and 2.4. The movement of the oxidation front and the swelling of the spark are shown in Fig. 2.1.

$$d_p(X) = d_{p,o}\sqrt[3]{z + (1 - X)(1 - z)} \tag{2.3}$$

$$d_{Me}(X) = d_{p,o}\sqrt[3]{(1 - X)} \tag{2.4}$$

Oxygen Transport across the oxide layer

One process that limits the oxidation reactions progress is the ability of metal and oxygen ions to diffuse through the oxide layer. For the oxidation of Iron by oxygen this oxidation process has been well studied [70, 78–80] and is often referred to as the parabolic rate law, because for a flat slab oxidizing at constant temperature the square of the weight gain or increase in oxide layer thickness from the reaction is equal to the product of parabolic rate constant, $K(T)$, and the time elapsed since the metal was exposed to the oxygen. For spherical particles the weight gain of the particle does not have the same relationship with the parabolic rate constant and the elapsed time because there are curvature effects and instead a slightly different approach must be used [77, 81], which we will use here. We start with the equation equating the rate of metal oxidation to the rate at which the oxide shell grows.

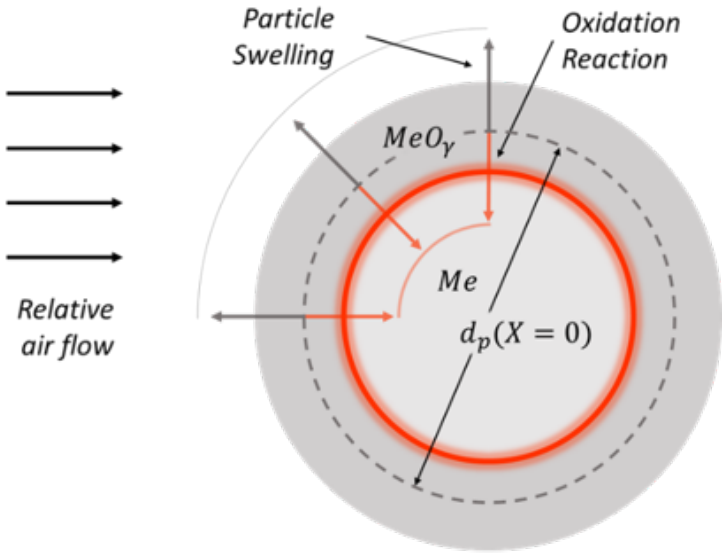

Figure 2.1: Illustration of the oxidation process inside the hot metal particle

$$\frac{d(m_{Me})}{dt} = \frac{8\pi K(T_p) d_{Me} d_p}{d_p - d_{Me}} \tag{2.5}$$

Where $K(T_p)$ is the parabolic rate constant which is given by Eqn. 2.6. The parabolic rate law accounts for the net rate of oxidation based on the diffusion of oxygen and metal ions towards each other.

$$K(T_p) = K_o exp\left(\frac{-E_a}{R_u T_p}\right) \tag{2.6}$$

In the case of Iron oxidation with air the activation energy, E_a, is $169452\ J/mol - K$, which is roughly the activation energy for Iron ion diffusion in FeO [70]. The value for the constant, K_o is $6.1 \cdot 10^{-4}\ m^2/s$. In addition to the explicit dependence on temperature the parabolic rate constant can also change with oxygen partial pressure [70].

The rate of metal consumption (Eqn. 2.5) can be directly related to the rate of oxygen consumption using the reaction (Eqn. 2.1). This results in Eqn. 2.7 which will be useful later.

$$\frac{d(m_{O,diff})}{dt} = \frac{\gamma M_O}{M_{MeO}} \frac{d(m_{Me})}{dt} \tag{2.7}$$

The consumption of oxygen according to this equation can be compared to the oxygen being delivered to the surface of the spark in the gas phase to determine which of the two processes is the one that will limit the oxidation.

Oxygen Transport in the surrounding air

Initially before a thick enough oxide layer forms, the reaction is dominated by the delivery of oxygen from the gas. For a spherical particle moving in a cross flow We can calculate the rate of oxygen delivery using a Sherwood number, Sh, correlation which relates the mass transfer to the surface of the particle to the diffusion of oxygen in the gas phase.

$$Sh = \frac{h_{MT}\ d_p(X)}{\rho_g\ D_{O_2/Air}} \tag{2.8}$$

Where

$$Sh = 2 + 0.6\ Re^{1/2}\ Sc^{1/3} \tag{2.9}$$

As given by [82] We know that $h_{MT} = \dot{m}^{"}_{O_2}/Y_{O_2}$, which we can directly relate to the rate of metal oxidation to get Eqn. 2.10.

$$\frac{dm_{O,conv}}{dt} = \pi d_p^2 h_{MT}\left[(Y_{O_2}\rho_{Air})\Big|_\infty - (Y_{O_2}\rho_{Air})\Big|_{surf}\right] \tag{2.10}$$

However if the oxidation process at the surface is very quick then the concentration of oxygen near the particle surface will be very small, causing Eqn. 2.10 to reduce to Eqn. 2.11

$$\frac{dm_{O,conv}}{dt} = \pi d_p (ShD_{O_2/Air})\Big|_{bl}(Y_{O_2}\rho_{Air})\Big|_\infty \tag{2.11}$$

Limiting Reactant for Oxidation

The amount of oxidation that will actually take place then will be the minimum of that predicted by Eqns. 2.7 and 2.11. We can then calculate the amount of metal consumed by the oxidation reaction and then express that relation in terms of, X.

$$\frac{\pi}{6} d_{p,o}^3 \rho_{Me}\frac{dX}{dt} = \frac{\gamma M_O}{M_{MeO}} min\left(\frac{dm_{O,conv}}{dt}, \frac{dm_{O,diff}}{dt}\right) \tag{2.12}$$

To elucidate the controlling physics of the coupled heat and mass transfer processes governing the oxidation of the sparks, we will non-dimensionalize the equations.

$$\frac{dX}{dt} = \frac{6(\rho_{Air}Y_{O_2})|_\infty D_{O_2}|_{bl} Sh}{\rho_{Me} d_{p,o}^2}\ min\left(\frac{dm_{O,conv}}{dt}, \frac{dm_{O,diff}}{dt}\right) \tag{2.13}$$

where $\xi = d_p(X)/d_{p,o}$, the non dimensional time can be defined as $\hat{t} = t/\tau_{HT}$ where τ_{HT} will be defined in the next section.

Oxidative Heating

The subsequent heating or cooling of the spark is dictated by sum of the heat generated by the oxidation process and the losses of heat by radiation and convective losses as shown in Eqn. 2.14

$$\frac{dT_p}{dt} = \frac{-\pi d_p^2}{m_p C_p}(\epsilon\sigma(T_p^4 - T_\infty^4) + h_{conv}(T_p - T_\infty)) + \frac{m_{p,o}Q_{ox}}{m_p C_p}\frac{dX}{dt} \tag{2.14}$$

where h_{conv} is given by the equations

$$Nu = \frac{h_{conv}\, d_p}{k_{air}} \tag{2.15}$$

$$Nu = 2 + 0.6\, Re^{1/2}\, Pr^{1/3} \tag{2.16}$$

and σ is the Stefan Boltzmann constant and ϵ is the emissivity and was set a a values of 0.8. The densities for Fe and FeO were assumed to be constant with respect to temperature and the specific heat capacities were calculated using Shomate polynomials from the NIST chemistry webbook [83] for both the metal and the oxide. The heat of reaction of the oxidation process, Q_ox was expressed in terms of energy released per unit mass of reacted Fe according to Eqn. 2.17

$$Q_{ox}(T_p) = H_{MeO_\gamma}(T_p) - H_{Me}(T_p) + \frac{\gamma}{2}H_{O_2}T_\infty) \tag{2.17}$$

0

Metal Spark Dynamics

Once the particles is ejected by the welder or the saw blade, the wind carries the particle in the wind direction due to the drag force that the air exhorts on the particle surface. At the same time gravity forces the particle downward toward the ground. The resulting particle trajectory is roughly parabolic and depends on the particles ejection velocity, the wind velocity, and the particle size and mass. The governing equations of the particle motion are those of momentum conservation in three dimensions. In vector form, they can be expressed as:

$$m_p\frac{d\vec{v}_p}{dt} = -m_p\vec{g} - \vec{F}_D \tag{2.18}$$

Where v_p is the velocity of a particle, with respect to the ground; and $\vec{x}_p$ is its position. The drag force on a particle is

$$F_D = \frac{1}{2}c_D\rho_{air}A_{proj}||\vec{v}_{rel}||^2\frac{\vec{v}_{rel}}{||\vec{v}_{rel}||} \tag{2.19}$$

Where $\vec{v}_{rel} = \vec{v}_{wind} - \vec{v}_p$ is the relative velocity between the particle and the air. The wind velocity, is assumed to have only horizontal components, orthogonal to the gravity vector, although its magnitude is a function of height above the ground. A_{proj} is the projected cross-sectional area

of the particle. The drag coefficient c_D is a function of the Reynolds number. The properties, such as the kinematic viscosity ν_{air} and the density of air ρ_{air} surrounding the particle, are evaluated at average conditions, which are taken to be the ambient pressure and the arithmetic mean of the spark temperature and the ambient temperature. It is assumed that all particles are spherical in shape. For low to moderate values of Re, we invoke an empirically matched approximation for the drag coefficient of a smooth sphere: Substituting the equation for the drag force, Eqn. 2.19 into Eqn. 2.18:

$$\frac{d\vec{v}_p}{dt} = \frac{C_D \rho_{air} ||\vec{v}_{rel}^2||}{2\ m_p} \frac{\vec{v}_{rel}}{||\vec{v}_{rel}||} - \vec{g} \tag{2.20}$$

$$\frac{d\vec{x}_p}{dt} = \vec{v}_p \tag{2.21}$$

Numerical Time Integration

The differential equations governing the motion of the particle, Eqns. 2.20 & 2.21 and ODE governing the particle temperature, Eqn. 2.14 and the particle oxidation, Eqn. 2.13. These eight ODEs can be solved simultaneously using a standard numerical ODE solver.

Model Inputs

In order to investigate the danger posed by these particles we will consider the scenario of a sparks produced on a structure $10m$ in above flat ground. The sparks were considered to be ejected at a 45° angle from the horizontal at a speed of 5.65 m/s. The particles are initially pure iron at a temperature of 1327°C. The incoming wind is follows at logarithmic profile from the ground as the profile described in [38] and has a strength of 13.4 m/s at 10 m from the ground. For this study we will only consider the scenario where that the wind is aligned with the direction of the ejection velocity of the particles/sparks, reducing the three dimensional problem into a two dimensional problem. The particles considered ranged from $1 - 7\ mm$. These particles are intended to span the range of particle conditions possible for welding, flame cutting, and abrasive cutting.

2.3 Results

Simulations of the trajectories and temperature-oxidation histories of iron particles are presented in Fig. 2.2 and Fig 2.3. In both figures the same conditions are simulated, with one case with the oxidation model active and another with the model deactivated to show the effect of the oxidation process.

It can be seen that the trajectory of the particle is not significantly altered by the oxidation process, as the lines of the oxidizing and non oxidizing particles are overlapping. Thus for the degree of oxidation and for the spark sizes presented here, we can then assume that the oxidation has a negligible effect on the trajectories of the sparks. The trend with landing distance and spark

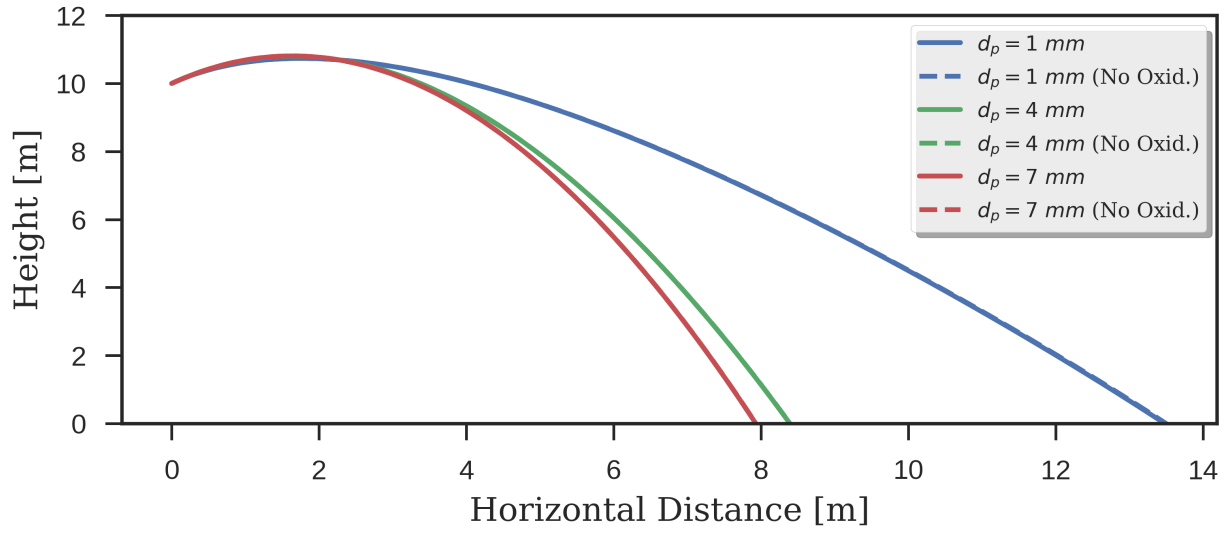

Figure 2.2: Trajectories oxidizing iron particles, with and without the oxidation model active. There is hardly a noticeable difference because the the oxidizing and non oxidizing particles for each size are almost exactly the same.

size is similar to the results found in a similar model by Tse et al. [38]. This trend occurs because the particles are in a flow field that is faster than their speed (at least initially) which will accelerate the particle. The magnitude of drag force which is accelerating the particle is roughly proportional to square of the particle diameter and the mass of the particle is proportional to the cube of the particle diameter. Thus the acceleration has an approximately inverse relationship with particle diameter.

The particle temperature and oxidation histories are shown in Fig. 2.3. It can be seen that the oxidation reaction causes the particles to initially experience a net heating and then a net cooling. When they land, the particles which oxidize have a temperature greater than their non-oxidizing counterparts. it is also observed that degree of self heating is most pronounced for the smaller spark sizes and similarly so is the subsequent cooling process. This is because the oxidation process and the heat losses scale with the square of the spark diameter while the thermal mass of the spark, $\approx \frac{\pi}{6} rho_p d_p^3 c_p$, scales with the diameter so that explains why the smaller particles heat up more but also cool the most.

The landing conditions of these simulations are presented in Table 2.1. The increase in the landing temperature increase is 100°C Elaborate on the table

To examine the details of the oxidation we will examine the equations which govern the oxidation and whether heating or cooling occurs. Graphs of filled contour plots of the instantaneous temperature derivative of the sparks is presented in Fig. 2.4 for different combinations of spark temperature and fraction oxidized.The black line in each subplot denotes where the temperature derivative has a value of 0. Thus the region of yellow-orange colors to the left of the black line is

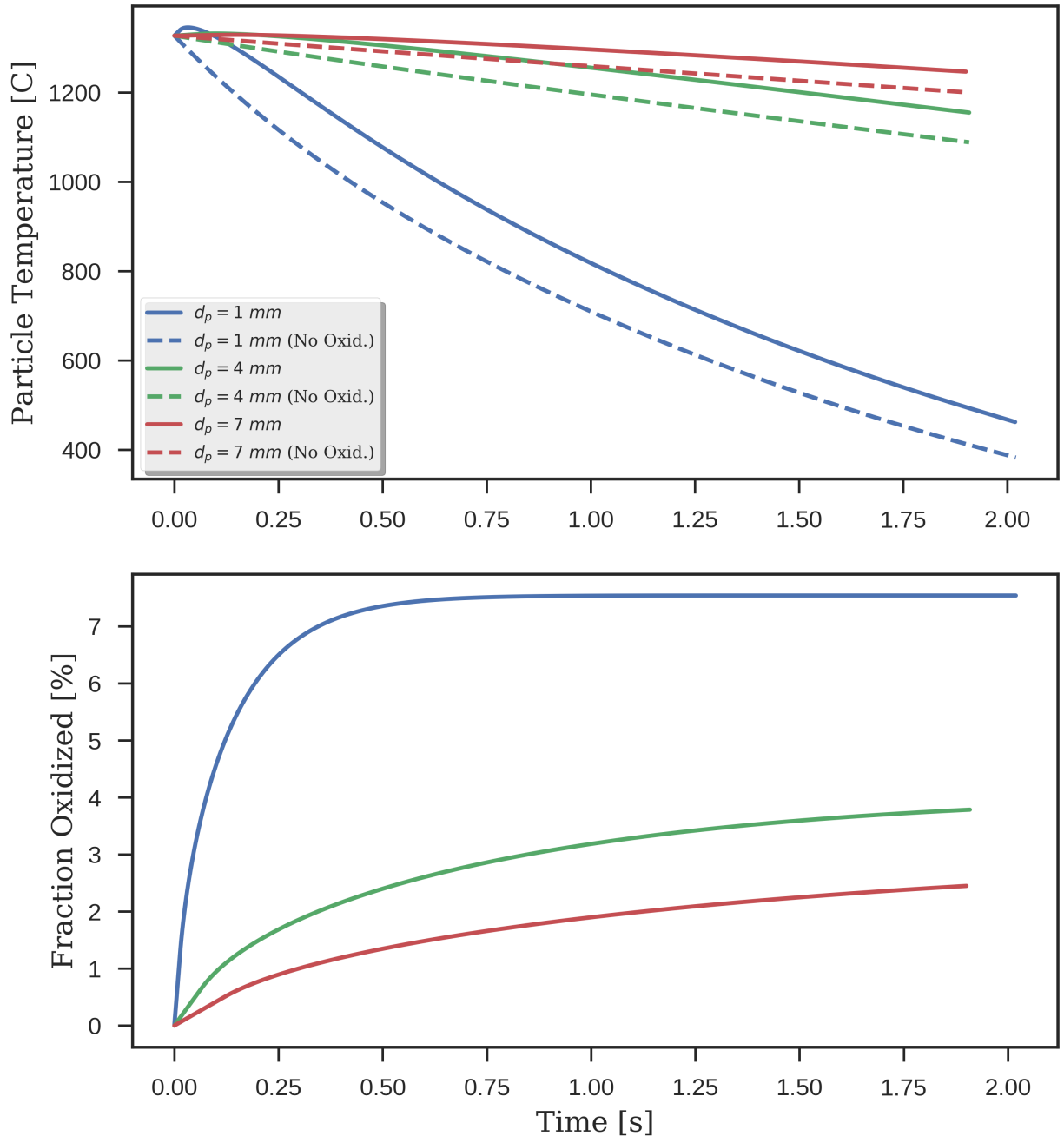

Figure 2.3: Temperature (top) and oxidation (bottom) histories of iron particle simulations with and without the oxidation model active. The oxidizing particles experience an initial heating and then cool. The smallest size is observed to stop oxidizing relatively early while the larger particles are still oxidizing marginally even at landing.

Table 2.1: Landing conditions of Simulations

Initial Diameter [mm]	Oxidation?	Final Temperature [C]	Landing Distance [m]	Fraction] Oxidized [%]	Landing Time [s]
1	No	382	13.51	-	2.02
4	No	1088	8.40	-	1.91
7	No	1200	7.94	-	1.90
1	Yes	462	13.48	7	2.02
4	Yes	1154	8.40	3	1.91
7	Yes	1246	7.94	2	1.90

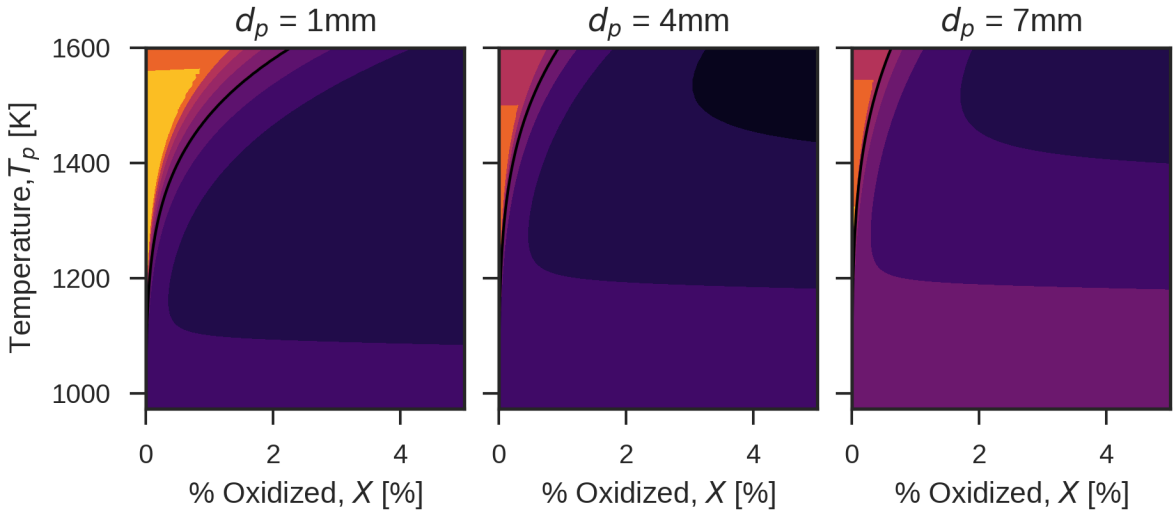

Figure 2.4: Filled contour plots of the the instantaneous temperature derivative of different sized particles for various particle temperatures and oxidation levels

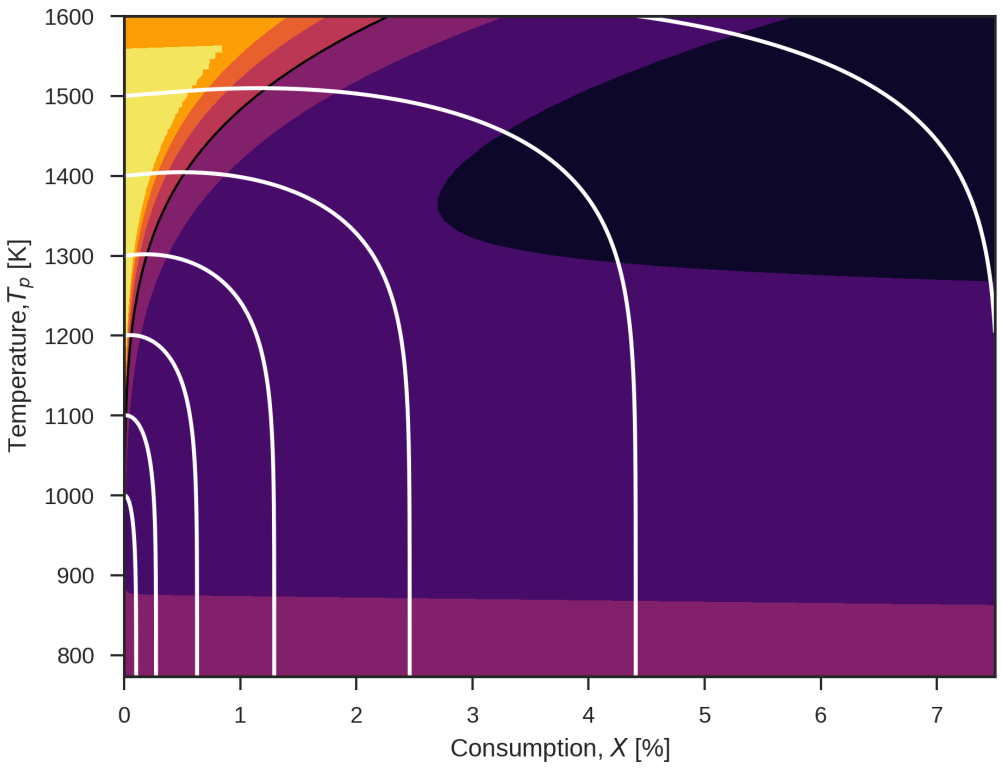

Figure 2.5: Steam plot of oxidation and heating, the white lines show paths that particles would take as they go through these states.

where sparks experience a net heating and the right with the dark purple colors the particle experiences a net cooling. We can see that the smaller particles are able to self heat at higher level of oxidation, X. We can also see that the maximum and minimum values of the temperature derivative are larger in magnitude for the 1 mm diameter graph, which is in agreement with the greater heating and cooling rates observed in the temperature histories.

To better illustrate how Fig. 2.4, corresponds to Fig. 2.3. A streamplot, showing the path in temperature - oxidation space that sparks would take. The case shown here is for a 1mm diameter spark. We can see that even after the sparks will still oxidize significantly when they are cooling. We see that the trajectories near the bottom of the figure become very steep, indicating that there is little oxidation occurring at that point and the spark is only cooling.

2.4 Discussion

The oxidation mechanism presented here is just one of the ways in which hot metal particles can be heated by a chemical reaction. Under the right conditions, particles can also undergo droplet burning [38] and heterogeneous combustion that for some reactions may and for others may not produce an oxide layer. The influence that these reactions and heat losses have on the ultimate hazard these particles/sparks pose as an ignition source is complicated. To better understand under what influence these processes have, the relevant timescales of the oxidizing spark can be be examined. These timescales include the time over which the particle/spark will cool appreciably, τ_{HT}, the time over which the spark will react, τ_{rxn} and, finally, the time it takes the spark to travel to the fuel of interest, $\tau_{motion} \approx (2h/g)^{1/2}$.

To determine the timescales for the oxidation of iron in air we will first non-dimensionalize the energy equation and the equation for the depletion of the unreacted iron, Eqns. 2.14 and 2.13, respectively. This will results in Eqns. 2.25 and 2.22

$$\frac{dX}{d\hat{t}} = \frac{\tau_{HT}}{\tau_{MT}}\,\xi\, min\left(1, \Xi\right) \tag{2.22}$$

where $\xi = d_p(X)/d_{p,o}$, the non dimensional time can be defined as $\hat{t} = t/\tau_{HT}$ where τ_{HT} will be defined in the next section. The mass convection based oxidation timescale τ_{MT} is given in Eqn. 2.23

$$\tau_{MT} = \frac{d_{p,o}^2 \rho_{Me}}{6\ Sh\ (Y_{O_2}\rho_{Air})\Big|_\infty} \frac{M_O}{M_{Me}\gamma} \tag{2.23}$$

and Ξ is given by Eqn. 2.24.

$$\Xi = \frac{\gamma M_O}{M_{MeO_\gamma}} \frac{8\rho_{MeO_\gamma} K(T_p) d_{Me}}{(d_p - d_{Me})(ShD_{O_2/Air})\Big|_{bl}(Y_{O_2}\rho_{Air})\Big|_\infty} \tag{2.24}$$

We then introduce the non-dimensional variable $\theta_p = (T_p - T_\infty)/(T_{p,0} - T_\infty)$ which after significant algebraic manipulation yields Eqn. 2.25

$$\frac{d\Theta_p}{d\hat{t}} = \left(\frac{1}{\xi^2 \hat{C}_p(X)}\right)\left(\frac{\lambda}{\xi}\frac{dX}{d\hat{t}} - \Theta_p\right) \tag{2.25}$$

where $\hat{C}_p(X)$ is the volumetric heat capacity of the particle as it changes composition, τ_{HT} is the time it takes for the particle to appreciably cool, given by Eqn. 2.26, and $\lambda = \frac{Q_{ox}(T_p)}{C_{Me}(T_p - T_\infty)}$ is a non-dimensional heat of reaction. While Eqn.2.25 appears complicated we can realize some things about the non-dimensional form that quickly simplify it. First the grouping ξ for iron varies between 1 and $z_{Fe}^{1/3} \approx 1.2$ and the grouping $\hat{C}_p(X)$, the ratio of the oxidizing sparks volumetric specific heat to that of pure metal, which varies between 1 and ≈ 1.5. Thus, while we can see that these parameters change during the oxidation process, the change does not cause more that a factor of 2.6 decrease in the temperature derivative.

$$\tau_{HT} = \frac{d_{p,o}^2 C_{p,Me}}{6\ Nu\ k_{Air}|_{bl}(1+\hat{Q})} \tag{2.26}$$

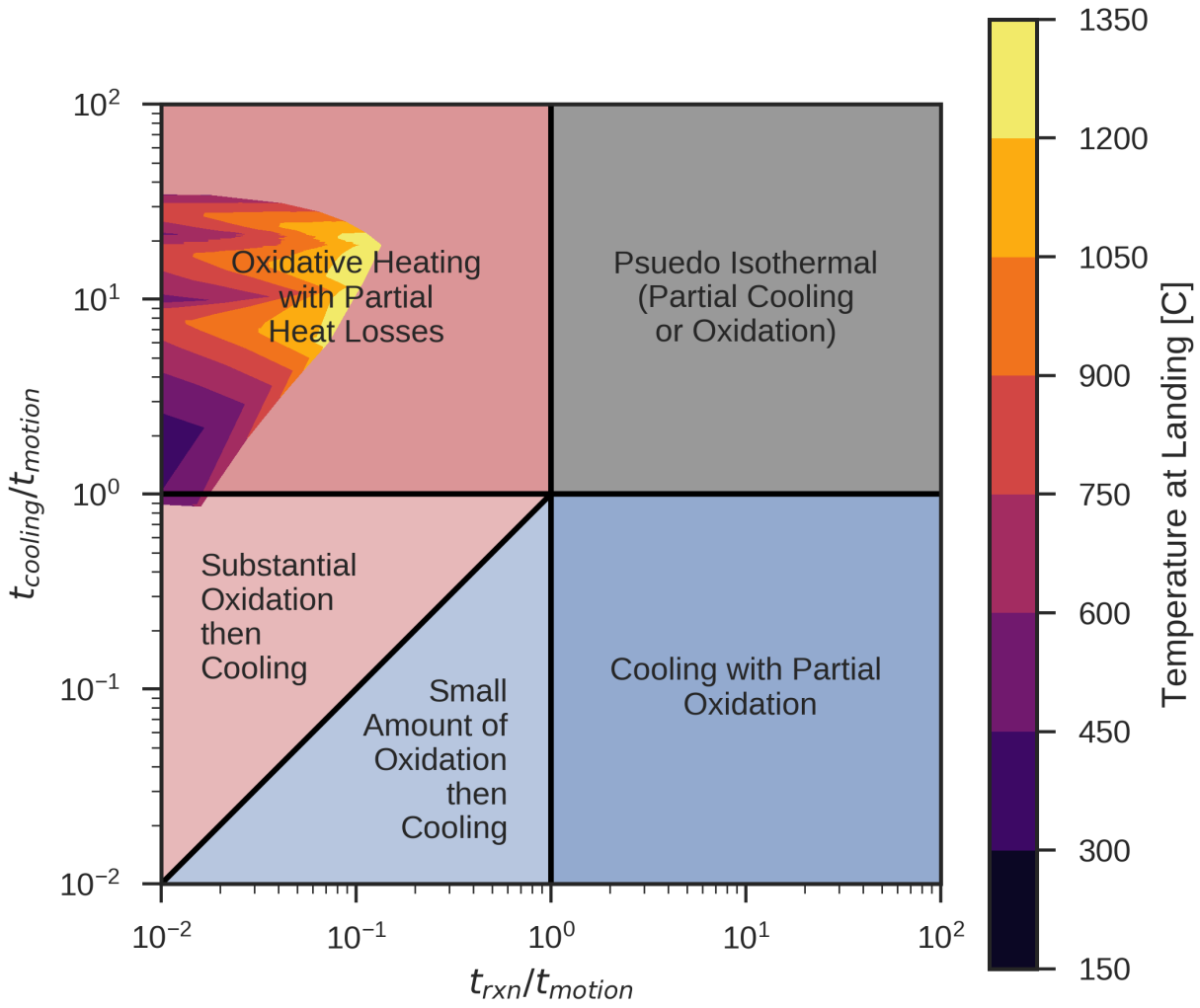

Figure 2.6: Plot showing qualitative behavior of oxidizing iron sparks in air with results of simulations superimposed as a filled contour plot showing landing temperature of the simulations. The horizontal and vertical axis are τ_{rxn}/τ_{motion} and $\tau_{cooling}/\tau_{motion}$ respectively

From these timescales we can calculate the time it will take to spark react, $\tau_{rxn} \approx \tau_{MT}$, the time it takes the spark to cool down to the ambient, $\tau_{cooling} \approx \tau_{MT} + \tau_{HT}$, and the time it takes for the spark to land, $\tau_{motion} \approx (2h/g)^{1/2}$. Comparing these timescales allows us to evaluate the importance of the oxidation reaction and heat losses on the sparks landing conditions. For

instance, if the reaction or heat loss timescales are considerably larger than the motion timescale then their effect on the temperature of the spark/particle might be negligible. The interaction of these timescales is somewhat complex and their interpretation for assessing the danger of the sparks also requires knowledge about the strength of the heating from the reaction and the magnitude of the heat losses. For the case of these oxidizing iron particles, Fig. 2.6 shows regions of different qualitative iron spark behavior in terms of $\tau_{cooling}/\tau_{motion}$ and τ_{rxn}/τ_{motion}. Then these timescales from simulations are superimposed as a filled contour plot. For the results in the filled contour plot, temperatures between 700°C to 1350°C.

We can see that the simulations of the oxidizing iron sparks are in the region where they should experience oxidation and then partial heat losses (larger sparks) and in some cases substantial oxidation then cooling (smaller sparks). This makes sense because in Fig. 2.5 we see the streamlines, which represent possible particle trajectories going past the black lines indicating that they experienced the full exothermic heating possible.

2.5 Conclusion

A metal oxidation model has been applied to a particle trajectory model which shows that iron particles can be heated to higher temperatures as they fly through oxidizing environments such as air. The heating these particles experience increases the hazard they pose to fuels as an ignition source. The oxidation is initially controlled by convective mass transfer of oxygen to the metal particles surface, then once a significant oxide layer builds up, diffusion of metal and oxygen ions in the oxide layer controls the oxidation process. Smaller particles experience greater heating than larger particles, but can also cool more quickly when the reaction is hindered by the oxide layer. Overall the oxidation reaction causes the metal particles to land at temperatures between 50 - 80 °C higher, depending on the particle size. Analysis on how timescales such as the reaction time, heat transfer time and time of motion (time until landing or contact with the fuel) were used to explain the thermo-chemical processes as the particle falls.

Combining models such as this one which simulate the trajectory sparks experience as well as the thermo-chemical change they experience with data from ignition experiments such as the ones later in this dissertation will allow us to predict the possibility of spot fires from welding processes. This will allow for more intelligent determination of clearance distances and work site regulations.

Chapter 3

Flaming Ignition of Cellulosic Powder by Hot Metal Particles

The ignition of natural combustible material by hot metal particles is an important ignition pathway by which wildland and urban spot fires are started. There are numerous cases reported of wild fires started by clashing power-lines or from sparks generated by machines or engines. Similarly there are many cases reported of industrial fires caused by grinding and welding sparks. In this work, the effect of metal type on the ability of hot metal particles to cause flaming ignition of powdered cellulose fuel beds is studied through laboratory experiments. The particle materials studied are stainless steel, aluminum, brass and copper. These metals are representative of clashing conductors (aluminum and copper) and those involved in machine friction and hot work such as welding (stainless steel and brass). The cellulose powder is used as a surrogate for natural fuel beds as cellulose is a major component of woody biomass. The metal particles tested ranged in size from 2 to 11 mm in diameter. They were heated to temperatures between 575 and 1100°C and dropped onto the fuel bed. Then the minimum initial particle temperatures required to cause flaming ignition were found for each particle size of each metal. The temperature required for ignition showed a hyperbolic relationship the particle size and temperature - the larger particles requiring lower temperatures to ignite the cellulose than the smaller particles. From these results, ignition boundaries were determined, separating conditions which are capable of ignition from those that are not. For large particles of all the metals, the ignition boundary is not very sensitive to particle size. For small particles the ignition boundaries are similar for the different metals and sensitive to both energy and temperature. The thermal properties of the metal play a lesser role in determining ignition with exception of the energy release from melting when it occurs.

This chapter is based on research previously published in the Proceedings of the Combustion Institute [49] and presented at the 2014 Fall Technical Meeting of the Western States Section of the Combustion Institute [84].

3.1 Experimental Apparatus

A schematic of the experimental apparatus is shown in Fig 3.1. The fuel bed is mounted in the bottom of the wind tunnel with the fuel bed surface flush with the bottom of the wind tunnel. The length of the wind tunnel is 550 mm with a cross section of 130 mm wide by 80 mm tall. The sample holder is 150 mm long, 100 mm wide and 50 mm deep with the leading edge 150 mm from the inlet of the wind tunnel. Laboratory air is flown through the wind tunnel with a centerline velocity of 0.5 m/s at the leading edge of the fuel bed.

As is mentioned above, the air flow velocity is a parameter of the problem that affects the rate of cooling of the particle and the generation of the flammable mixture near the particle; in this study the air flow velocity was held constant. The air velocity used was chosen because it produces a regular flow without disturbing the powdered cellulose surface. Because of the low flow velocities, the ignition conditions found in this work may not be representative of those that would be obtained at higher velocities. Flow uniformity is reduced when the tunnel top is opened to introduce the particles. To overcome this complexity and ensure a uniform cross-flow velocity between tests, particles were only dropped on the leading half of the fuel bed. The relative humidity and temperature of the flow were measured daily and found to be on average $39.2\% \pm 7.9\%$ and 24.0 ± 2.0°C respectively. Viewing windows in the sides of the tunnel allow optical access for video recording of Schlieren images. The Schlieren system utilizes a double pass configuration with a color bullseye (blue center, yellow and red rings) and a spherical mirror with a focal length of 1 m. Videos were recorded at 1200 frames per second using a digital camera. A high temperature electrical tube furnace is used to heat the metal particles. A linear guide holds a ceramic spoon approximately 140 mm above the fuel bed. This guide is collinear and concentric with the tube furnace such that the spoon can easily be inserted and removed from the furnace. A type K thermocouple is embedded in the spoon to provide a reliable measurement of the particle temperature. The metal particles are left in the furnace until their temperature reaches equilibrium conditions as indicated by the thermocouple placed in the ceramic spoon. It should be noted that the particle temperature reported here is that of the particle in the oven, not at landing. The particle temperature at landing is obviously lower and dependent on the particle size, temperature and emissivity. Estimation of the temperature reduction during the particle drop is no more than 50°C for any test. This estimation was done by calculating the heat losses from convection and radiation and assuming the inside of the particle was thermally uniform.

The fuel bed is powdered cellulose, which was chosen because it is chemically homogeneous and the major component of woody biomass. The individual grains of cellulose in the powder have a mean diameter of 0.36 mm and at least 80% are 0.42 mm or smaller according to manufacturer (Sigma Aldrich) documentation. The average bulk density of the fuel beds was $338 \pm 40\ kg/m^3$. The cellulose settled volume was held constant for all experiments. The settled volume refers the minimum volume occupied by the fuel bed after vigorous vibration. The fuel was laboratory-conditioned and the fuel moisture content of the fuel was measured each day tests were conducted. This involved drying lab-conditioned samples in an oven at 110 ± 5°C for at least 4 hours. Each sample weighed at least 1.3 g and the mass was measured before and after drying. The average moisture content for each day was $7.0 \pm 2.0\%$.

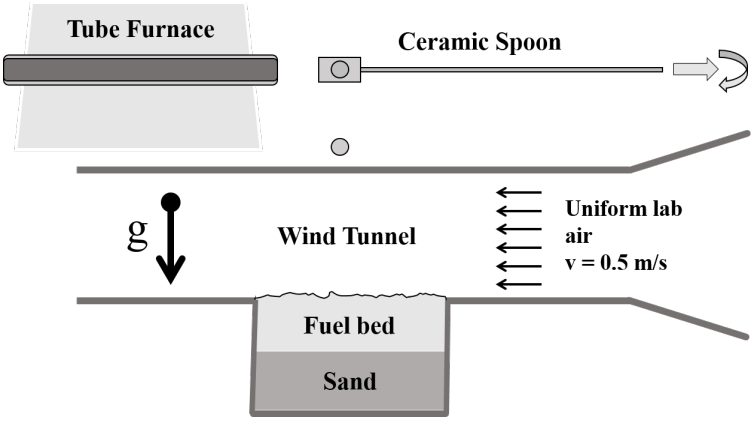

Figure 3.1: Schematic of Experimental Apparatus

For this study, metal particles composed of Stainless Steel 302, Aluminum 1100, Brass 260, and Copper 110 were used. The metal particles studied were either spherical or approximately spherical in shape. The particles ranged in size from 2 to 11 mm in diameter. The temperatures tested ranged from $575 - 1100$°C. The maximum particle temperature was limited by the maximum operating temperature of the tube furnace. For the range of particles tested no ignition was observed at 575°C, so further tests were not conducted below that temperature. Tests using brass and copper were limited to temperatures below their melting points (915°C and 1065°C, respectively) because when these metals were heated past their melting point the molten particle would stick to the ceramic spoon. There was no commercially available coating found which would prevent this from occurring in an oxidizing environment. As such the maximum temperature used for brass was 900° C and 1050° C for copper. The relevant thermal properties for the materials are shown in Table 3.1.

Table 3.1: Thermal properties of Stainless Steel 302, Aluminum 1100 (solid and liquid properties), Copper 110 and Brass 260.

Particle Material	Stainless Steel 302	Aluminum 1100 (molten)	Copper 110	Brass 260
Melting range [$^\circ C$]	1400-1420	643-657	1065 - 1083	915-955
Heat of Melting [kJ/m^3]	2122	1057	1822	1433
Density [kg/m^3]	7860	2710 (2375)	8890	8530
Heat Capacity [$J/kg{\cdot}K$]	500	900 (1141)	385	375
Thermal Cond. [$W/m{\cdot}K$]	21.5	220 (90.7)	390	120

At least five tests were conducted for each particle material at a given diameter and temperature. In order to minimize the effects of random variations in the fuel beds and the penetration of the particle into the fuel bed, the location where the particle was dropped was varied and no more than three tests were done on a single fuel bed. As was mentioned in the introduction, the problem

has several parameters that can affect the ignition process. However, we feel that the experimental conditions are well controlled and that five tests is sufficient data sampling to provide accurate results, particularly since they are supported by the physics underlying the ignition problem.

3.2 Results

The primary objective of this work is to identify the temperature at which the metal particles of a given size and material will cause flaming ignition of the powdered cellulose. During flaming ignition events, the flame would initiate nearby the hot particle and the heat generation would be sufficient to allow the flame to propagate across the free cellulose surface. The experimental results are shown in Figure 3.2. Each of the sub-figures (a-d) corresponds to all of the tests conducted with a particular metal. The circles on the figure each correspond to a set of at least five tests conducted with a particular diameter and temperature particle. The color of the circles follows a colormap which denotes the fraction of those tests that resulted in flaming ignition. Thus a completely black circle corresponds to test conditions where flaming ignition was never observed and a white circle corresponds to a test condition where all of the tests ignited. Intermediate values correspond to the colors shown on the color bar in the center of the figure. Boundaries are provided indicating approximately 5% probability of ignition.

The results for the different materials follow a similar trend. There is a hyperbolic relationship between the temperature and particle size, with the larger particles requiring lower temperatures to ignite the fuel than smaller particles.

3.3 Discussion

Ignition Phenomenology

Following completion of the experiments, high-speed videos of each of the tests were analyzed. The videos of tests where flaming ignition occurred for every test provide qualitative insight to the processes that are occurring during ignition. Specifically it can be seen that there is different behavior between tests with very small, high temperature particles and tests with large, relatively low temperature particles. This is illustrated in 3.3, which shows the flaming ignition events of two particles, one with a diameter of 9.53 mm and heated to 675°C shown on the left and a 4.76 mm particle heated to 900°C shown on the right.

In the cases with larger particles at lower temperatures, a dark plume is observed emanating from around the particle at some time after the initial impact, as is show in the images of 3.3-a. A dark appearance in a Schlieren image means an object is opaque, suggesting either grains of cellulose powder are lofted by the particle's impact or heavier products of pyrolysis vapor are present. The current resolution of the videos (0.22 mm) means that the presence of small lofted cellulose grains cannot be resolved. However, it should be noted that in the cases of bouncing particles (such as the test shown in of Figure 3.3-a) the plume appears to track the particle, which

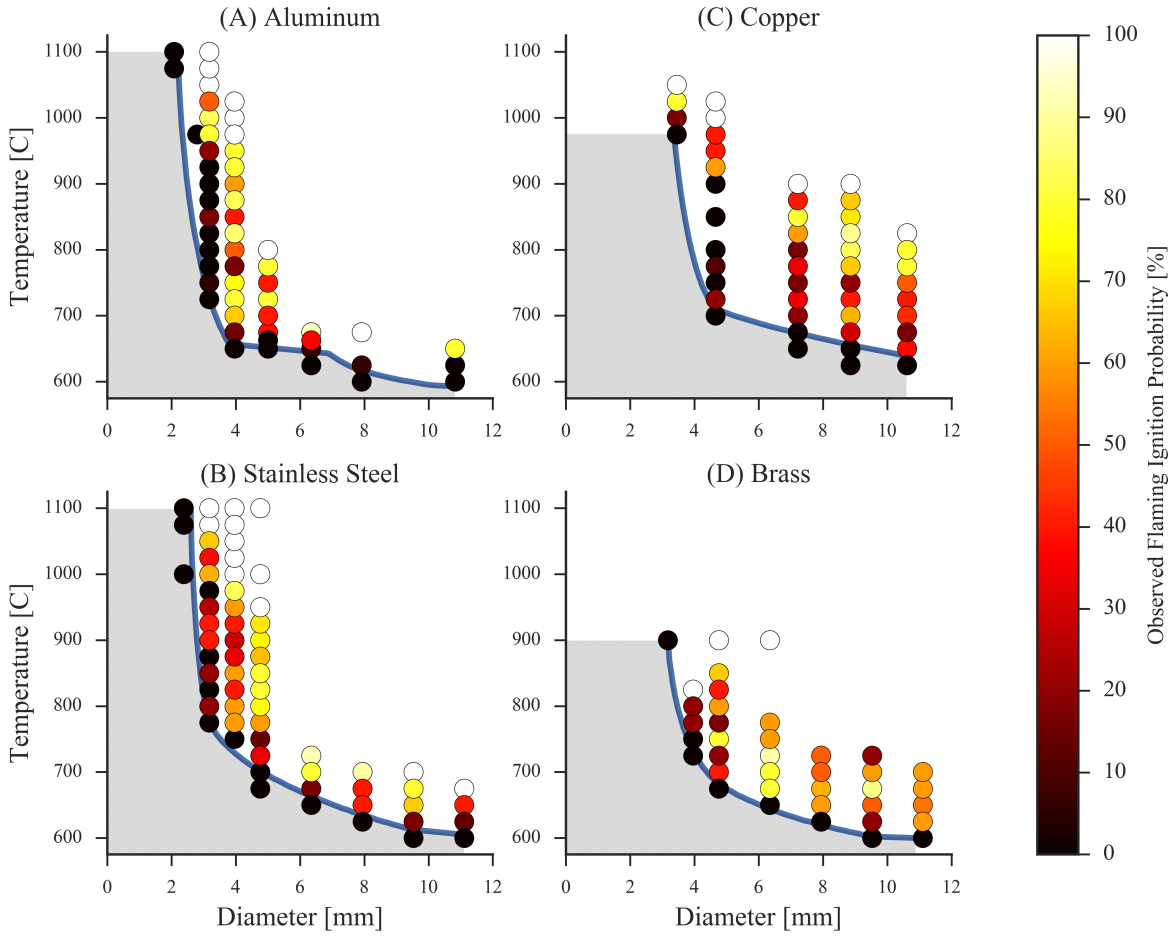

Figure 3.2: Observed ignition probabilities for particles of all four metal types.

seems nonphysical for particles lofted by impact. Assuming the cloud is fluid in nature, it seems likely that the opacity is due to condensed pyrolysis products.

For the tests with small particles at higher temperatures, we see from the top image of 3.3-b, that the pyrolyzate plume produced from the impact site of the particle is transparent, unlike that of a large diameter particle. This is in contrast to the larger and more violent expansion observed with larger particles, suggesting larger particles pyrolyze more fuel than required prior to the ignition event.

Parameters Controlling Ignition

To analyze the results in Figure 3.2 it is useful to describe phenomenologically the thermo-chemical process underlying the ignition of the combustible fuel bed by a hot metal particle. Once in con-

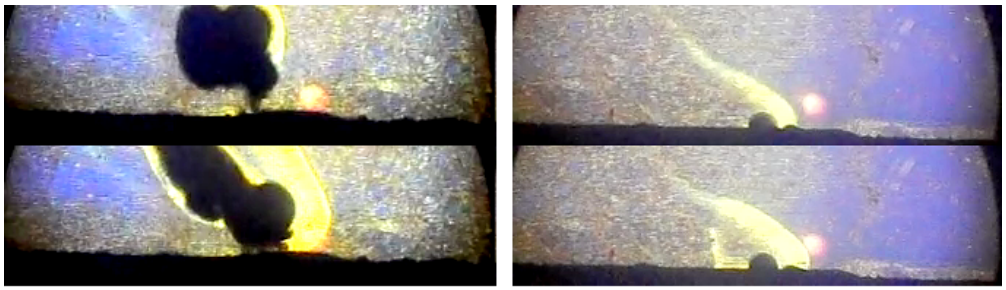

(a) 9.5 mm Steel particle intially heated to 675°C

(b) 4.8 mm Steel particle intially heated to 900°C

Figure 3.3: Schlieren Images Prior to and During Ignition: Note that the larger particle produces a dark, opaque cloud of pyrolyzate in the first frame while the small particle produces a transparent plume of pyrolyzate. The small bright circle that appears near the lower middle of all frames is an artifact of the Schlieren imaging technique and is not related to the ignition process.

tact with the fuel bed the metal particle must transfer its energy to the fuel so that it heats up and pyrolyzes enough material to create a flammable mixture of pyrolyzate and air around the metal particle. In this process the particle temperature decreases as its energy decreases (note that energy is also lost to the surrounding environment). After the flammable mixture is formed, it will ignite if the heat generated by the gas phase reactions can overcome losses to the environment. If the gas phase reactions can produce enough heat to offset the heat losses gas phase ignition may occur. If the surface of the metal particle is hot it can provide heat to the flammable mixture which can help it ignite. There do appear to be qualitative differences between the ignition by small-hot particles and the large-cool particles. The large particles near the ignition boundary produced substantial amounts of opaque pyrolyzate and the subsequent ignition events were much more vigorous and sometimes even audible. For the small particles near the ignition boundary, there was minimal observable pyrolyzate and ignition appeared in the gas phase farther away from the particle surface.

From the data shown in Figure 3.2 it is clear that there is different behavior between very large and very small particles for all of the materials studied as with similar studies [3, 46, 48, 51, 52]. Figure 3.4, shows the ignition boundaries for each of the four metals. The differences with previous results from the author's laboratory [46, 51] for steel and brass particles are due to subsequent improvements in the determination of the particle temperature for both and differences in the effect of the fuel bed density [46]. The bulk density of a porous fuel will effect the flow and availability of oxygen [85]

From Figure 3.4 it can be seen that all the metals show similar minimum ignition temperatures for a given diameter, despite large changes in the different metal's thermal properties, such as the particle's density, heat capacity, and thermal conductivity. For larger particles the minimum ignition temperature is not very sensitive to particle size. This seems to indicate that particle energy has a lesser role in the ignition process than the surface temperature, for larger particles since the physical properties of the materials are different and the energy is proportional to the particle

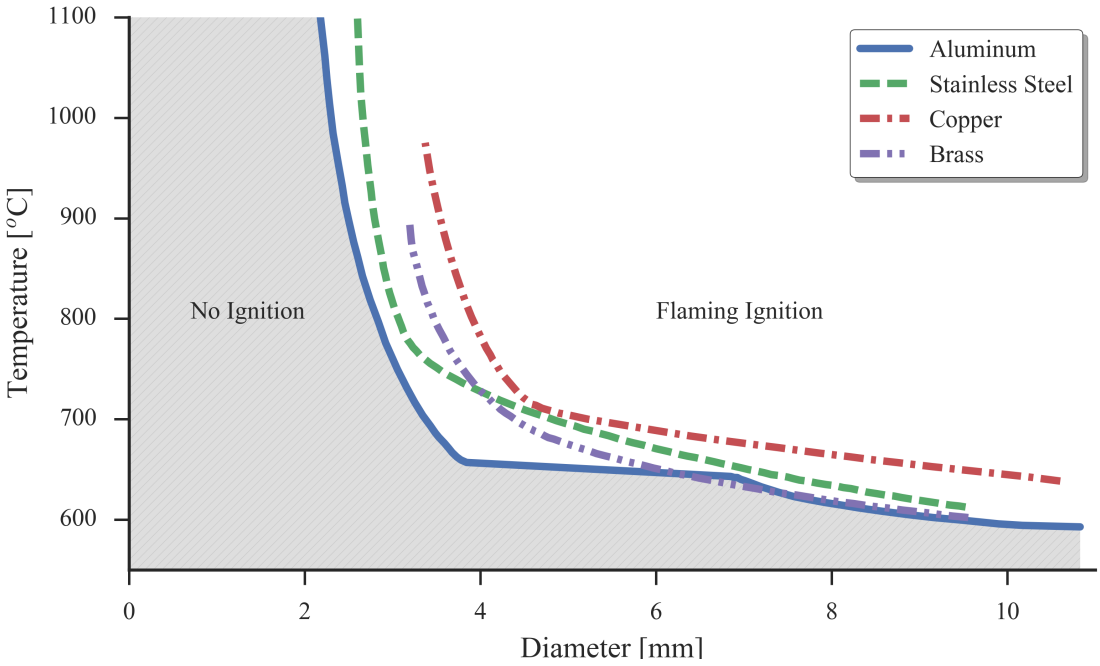

Figure 3.4: No ignition limits of the four metals tested with the ignition limits for comparison

volume. For small particles it is seen that the temperature required to achieve ignition is very sensitive to size of the particle. This indicates that the particle energy has a more important role in the ignition process than the particle temperature for small particles since small reductions in diameter requires large temperature increases. Furthermore if we examine the curves corresponding to aluminum and stainless steel in Figure 3.4, we see that 4 mm particles of aluminum ignite at temperatures roughly $100°$C lower than their stainless steel counterparts, but the energies of the two particles are actually very similar as shown in Figure 3.5. The energy values shown in Figure 3.5 were calculated assuming constant material properties for each material phase. The energy released from melting was treated as a linear variation over the melting temperature range. The energy values were calculated as energy above the ambient temperature.

Furthermore, examining the aluminum ignition boundary in Figure 3.4 it can be seen that there is a sharp corner at a diameter of approximately 3.5 mm. Between 4 mm and 7 mm diameter the ignition limit follows the melting temperature range and for diameters greater than 7 mm the ignition limit drops below the melting temperature. This indicates that melting has a significant effect on the potential for the particles to ignite for diameters greater than 3.5 mm. One possible explanation for this is that the molten particles have considerably greater energy than particles that are not molten. When comparing the volumetric heat of melting to the volumetric heat capacity (the product of ρ and c_p), it is seen that the latent heat of melting adds energy equivalent to the energy gained from heating the aluminum particle an additional $433°$C. Thus, a completely molten particle

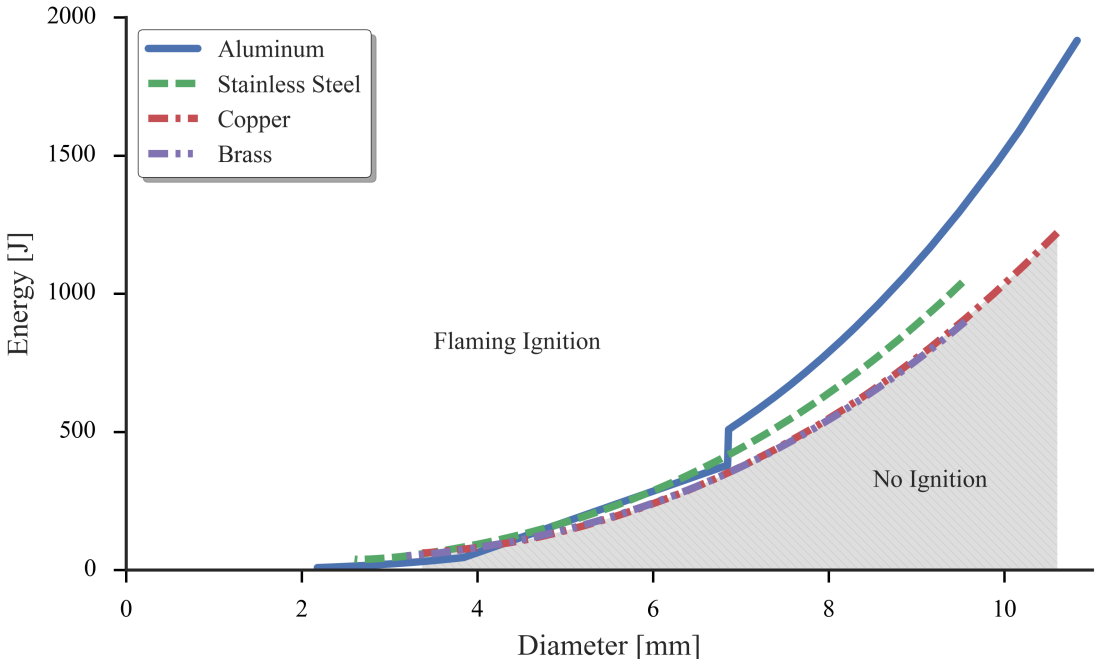

Figure 3.5: Bulk initial energy vs. particle diameter along the flaming ignition boundary

has considerably more energy than a barely molten particle despite the temperature difference of only $15°$C. For particles smaller than 3.5 mm the aluminum particles behave more and more like the stainless steel particles indicating that the contribution from the melting energy is not large enough and thus higher temperatures are needed to provide the required energy to ignite the fuel.

Copper exhibits some noticeable deviation in ignition behavior from the other metals, specifically copper particles require larger temperatures to ignite than the other metals. It is worth noting that at temperatures above the liquidus temperature of aluminum, $657°$C, copper has thermal properties drastically different from the other metals. Both the thermal conductivity and thermal diffusivity are at least a factor of three larger than the other materials in that range. This would allow increased heat transfer from the metal particle to the cellulose, but would also mean faster transient temperature changes. As a result, copper particles may be unable to retain heat long enough for a nascent gas phase reaction to become self-sustaining. Based on the higher temperatures required for ignition, it seems as though this latter effect is more prominent.

The present ignition results together with those in [52] and [46] show that the bulk energy alone is not the determining factor for ignition to occur. From Figure 3.5, it is seen that energy alone does not dictate ignition. Specifically, small particles with small bulk energy can ignite the cellulose, while large particles with considerably higher energies cannot ignite the cellulose unless they have a sufficiently high temperature. For example, a 10 mm particle with an initial temperature of $600°$C has approximately 6 times the energy of a 4 mm particle at $1100°$C and yet

the smaller particle will ignite and the larger particle will not. Based on the assumption that some minimum amount of gaseous fuel is required to initiate a combustion reaction, it seems there must be some minimum energy requirement. However, this appears to be a necessary, but not sufficient, condition for ignition.

As was proposed in [53], the exact role of particle temperature and diameter in determining ignition remains unclear. One possibility is that the classic balance of heat generation and heat losses, as proposed by Silver [86] in his study of gaseous mixture ignition by hot particles, also applies to solid fuels. In his analysis, Silver [86] proposed that ignition would occur when the heat generated by the incipient combustion reaction in a thin layer around the particle is greater than the losses to the particle and the surroundings. Ignition of a solid fuel is clearly more complicated; because of the higher density of the solid fuel, time is needed for pyrolysis, and the transport and mixing of the pyrolyzate with the oxidizer [87]. During this time, the particle, and the system in general, are losing heat through convection and radiation. In the time required for mass transport to occur, very large particles would lose less heat due to their large thermal mass, and only a sufficiently high initial temperature would be necessary for ignition. Very small, high conductivity particles would lose heat much more rapidly, and thus both a sufficient initial temperature and thermal mass would be required such that the particle and surrounding gases had not cooled off too much during the mass transport time. This would also explain the apparent increased sensitivity to randomness for smaller diameters and high conductivity metals, as both the mixing time and heat losses during that time would be affected by things like impact dynamics, local fuel bed density, and local flow conditions.

3.4 Conclusion

Tests on the flaming ignition of powdered cellulose fuel beds have been performed over a large range of particle sizes and temperatures for metals of various thermal properties. These metals are representative of potential sources of ignition of natural fuels in practical situations. For large particles of all of the materials, ignition behavior appears to be very sensitive to temperature, but sensitivity to temperature appears to decrease as the size is decreased. The data indicates that the energy of the metal particle plays an increasingly important role for determining ignition as particle size is decreased. However, initial metal particle's energy was shown to be an insufficient indicator of ignition likelihood. Ignition was observed in the gas phase and differences were noted in the behavior of small and large particles. Specifically, large metal particles tended to produce heavier pyrolyzate products and ignite violently, whereas small particles produced very little heavier products and ignited in a more subdued fashion. Overall it was found that, except for copper, the thermal properties of the material did not have a strong effect on ignition except for the effects from melting. The process of melting allows the particles to store more energy at high temperatures and increases their ability to ignite, however neither energy nor temperature have proven to be the sole factors controlling ignition.

It has been shown that the problem of the ignition of a solid fuel bed by a hot metal particle, spark or ember is very complex, involving solid and gas phase thermochemical processes together

with geometric and ambient effects. The effects of parameters such as fuel bed composition and moisture content, air flow velocity and properties, particles interaction and accumulation, among others, will affect the ignition boundaries reported in this work. However we feel that the present results provide a good basic understanding of the ignition of fuel beds by hot metal particles. It also provide a data base for verification of theoretical models of the process.

Chapter 4

Flaming Ignition of Natural Fuels by Aluminum Particles

The ignition of combustible material by contact with hot metal particles is an important pathway by which wildland and urban spot fires are started. This work examines how fuel characteristics such as density, morphology and chemical composition effect the ability of the fuel to be ignited by a hot metal particle. Fuels were prepared out of three materials: alpha-cellulose, a barley/wheat/oat grass blend, and pine needles. Each material was prepared as a powder and as larger, long pieces: strips of cellulose paper, loose grass, and pine needles. These fuels are representative of thermal insulation (cellulose strips), dry grasses (grass blend), forest litter (pine needles) and duff (powders). Aluminum particles ranging from 2 - 8mm in diameter heated to temperatures between 575 - 1100°C were dropped onto these fuels. The particle temperature required for ignition becomes higher as the particle size decreased. The results show that the required temperatures for ignition of powders were lower, with this trend particularly pronounced for the alpha-cellulose fuels. The biomass fuels required higher temperature particles to ignite, indicating that the presence of other ligno-cellulosic materials make ignition more difficult. The results show that powders were capable of ignition at lower temperatures, particularly with the alpha-cellulose.

This chapter is based on research presented at *The* 10^{th} *Asia-Oceania Symposium on Fire Science and Technology* held in Tsukuba, October, 2015 [88] and at the *Fire and Materials Conference* in San Francisco [89].

4.1 Experimental Apparatus and Methods

Experimental Apparatus

The experimental apparatus used was the same as the one described in Chapter 3. The mean and relative humidity and temperature of the air flow were measured daily and found to be on 16.2% $\pm$ 4.2% and 26.6 $\pm$ 3.3^{o}C respectively.

Table 4.1: Fuel Bed Properties

Fuel	Density [kg/m^3]	MC [%]	Chemical Composition	d_{char} [mm]
Cellulose Powder	344 ± 36	7 ± 1	100% α-cellulose [92, 93]	0.4 [93]
Cellulose Strips	42.5 ± 0.1	7 ± 1		5
Pine Needle Powder	370 ± 19	8 ± 1	30% α-Cellulose 20% Hemi-cellulose	0.5
Pine Needle	57 ± 1	8 ± 2	26% Lignin [94]	2
Grass Blend Powder	282 ± 1	7 ± 2	36-43% α - Cellulose 23-28% Hemi-cellulose	0.5
Grass Blend	75 ± 1	8 ± 2	7-18% Lignin [95, 96]	7.5

Fuel Beds

The fuels tests were composed of three different fuel materials (alpha-cellulose, a grass blend of barley/wheat/oat, and dead pine needles). These three fuel materials were prepared in two different morphologies for a total of six different fuels, shown in Fig. 4.1. The first morphology was a powder with powder grains small enough to pass through a 500-mesh sieve conforming to ASTM E-11 [90], this type of mesh allows particles that fit through 0.5 mm by 0.5 mm openings in a larger sieve to ensure a given particle size. The second morphology tested had a lighter bulk density than the powder morphology and the size of the individual pieces of the fuel were much larger. The cellulose strips, pine needles and the grass blend where cut to lengths between 37.5 and 87.5 mm and were typically $\sim$7.5mm wide for the grass blend and $\sim$5mm for the cellulose strips. The diameter of the pine needles was found to be $\sim$2 mm. The pine needles were collected from litter under a ponderosa pine (Pinus ponderosa) on the University of California Berkeley campus and then dried, cut to the specified length, and then conditioned in the laboratory. The grass blend was obtained commercially from Alfalfa King [91], and then cut to the specified length. The grass blend and its powder were dried in an oven and then allowed to reach an equilibrium moisture content comparable to the cellulose fuels ($\sim$7%). Rough values of expected compositions of the grass blend and pine needles were made by examining values reported in the literature for the oats, barley, and wheat grasses. Specific values of the moisture content and chemical compositions are shown below in Table 1. The cellulose strips were cut uniformly to the same length range and had a thickness of 5mm and were cut from alpha cellulose ashless paper [92]. The different fuel compositions allow us to examine the effect of hemi-cellulose and lignin content which is removed from the woody biomass to produce α-cellulose. The relevant fuel properties are shown below in Table 4.1.

The α-cellulose was chosen as a reference fuel bed material for its chemical homogeneity and because it is the largest component of woody biomass. The grass blend of barley, wheat, and oat

Figure 4.1: Photographs of the six fuels tested

grasses was chosen as representative of grassy fuels. The pine needles were chosen because they are representative of pine forest litter. In all experiments with powdered fuel beds, the settled volume was held constant. The settled volume refers to the minimum volume occupied by the fuel bed after vigorous vibration. The fuel beds were laboratory-conditioned and the moisture content of the fuel was measured each day tests were conducted. This involved drying laboratory-conditioned samples in an oven at 110 ± 5^{o}C for at least 4 hours. Each sample weighed at least 1.3g initially and the mass was measured before and immediately after drying. For this study, aluminum particles composed of aluminum alloy 1100, an alloy used for overhead power transmission in the United States, were heated in the tube furnace, and dropped onto the various fuels. The metal particles studied were either spherical or approximately spherical in shape. The particles ranged in size from 2 to 8 mm in diameter. The temperatures tested ranged from 525 - 1100^{o}C. Higher temperatures were not performed because 1100^{o}C was the maximum operating temperature of the tube furnace. For the range of particles tested, no flaming ignition events were observed at 525^{o}C, so additional tests were not conducted below that temperature. The relevant thermal properties for aluminum 1100 in both the solid and molten states are shown in Table 4.2

The goal of these experiments was to provide a boundary where flaming ignition will occur. To achieve this, work was focused only on the boundaries where flaming ignition occurred and where it did not occur. Test conditions were chosen to focus on finding the lowest temperature where flaming ignition could occur for a given size particle and a given fuel bed. This was achieved by performing guess tests at increasing temperatures, in multiples of 25^{o}C until an ignition event was

Table 4.2: Aluminum Particle Thermal Properties

Phase	Solid [97]	Molten [98–100]
Density [kg/m^3]	2710	2375
Specific Heat [J/kg·K]	900	1141
Thermal Conductivity [W/m·K]	220	90.7
Heat of melting [kJ/kg]	390	390
Thermal diffusivity [m^3/s]	$9.02{\cdot}10^{-5}$	$3.35{\cdot}10^{-5}$
Melting Temperature [^{o}C]	643 - 657	

observed. Then tests were performed at the temperature 25^{o}C lower than the lowest temperature where ignition was observed until either 5 tests were performed that did not result in ignition or an ignition event was observed. In this case the temperature was lowered by 25^{o}C and the process was continued recursively until a temperature was found where none of the 5 tests performed resulted in flaming ignition. For this study the tests could have one of two possible outcomes: flaming ignition or no ignition. Tests were designated flaming ignition if a flame was visible for at least one second. Flaming ignition happened in less than 1 second for all flaming ignition events observed. To minimize the effects of random variations in the fuel beds and the penetration of the particle into the fuel bed, the location where the particle was dropped was varied and no more than two tests were done on a single fuel bed on a given day. Although it is difficult to eliminate the randomness of the process, we feel that the experimental conditions were well controlled and that five tests were a good data sampling to provide an accurate measure of the ignition boundary.

4.2 Results and Discussion

The results from the experiments and the flaming ignition boundaries for the six fuels tested are presented in Fig. 4.2. Each of the sub-figures (a-f) of Fig. 4.2 corresponds to the tests conducted with one of the fuels. The circles correspond to sets of at least three tests for non-black circles and five for black circles and were colored based on the fraction of the experiments that resulted in a flaming ignition. Thus, black circles denote cases were FI was never observed and white circles to tests were flaming ignition occurred every time, intermediate values were colored per the colorbar at the right of the figure. The black circles were used to determine the ignition boundaries presented in Fig. 4.2. The flaming ignition boundaries denote a barrier separating conditions which can initiate a flame from those conditions which cannot. The ignition boundaries provide a good metric for comparing the ignition hazards of the different fuel relative to one another. It should be noted that in the case of the grass blend powder, many of the events that did not result in flaming ignition resulted in smoldering ignition, unlike the other fuels. The data regarding smoldering ignition is not presented here, but is discussed in Chapter 5 and [50]. Overall there are some common features among the results from the different fuels. The FI boundaries show monotonic rises in required particle temperature for ignition as the particle size decreases. While most of them have a similar hyperbolic shape, the ignition boundary for alpha-cellulose has a region that is

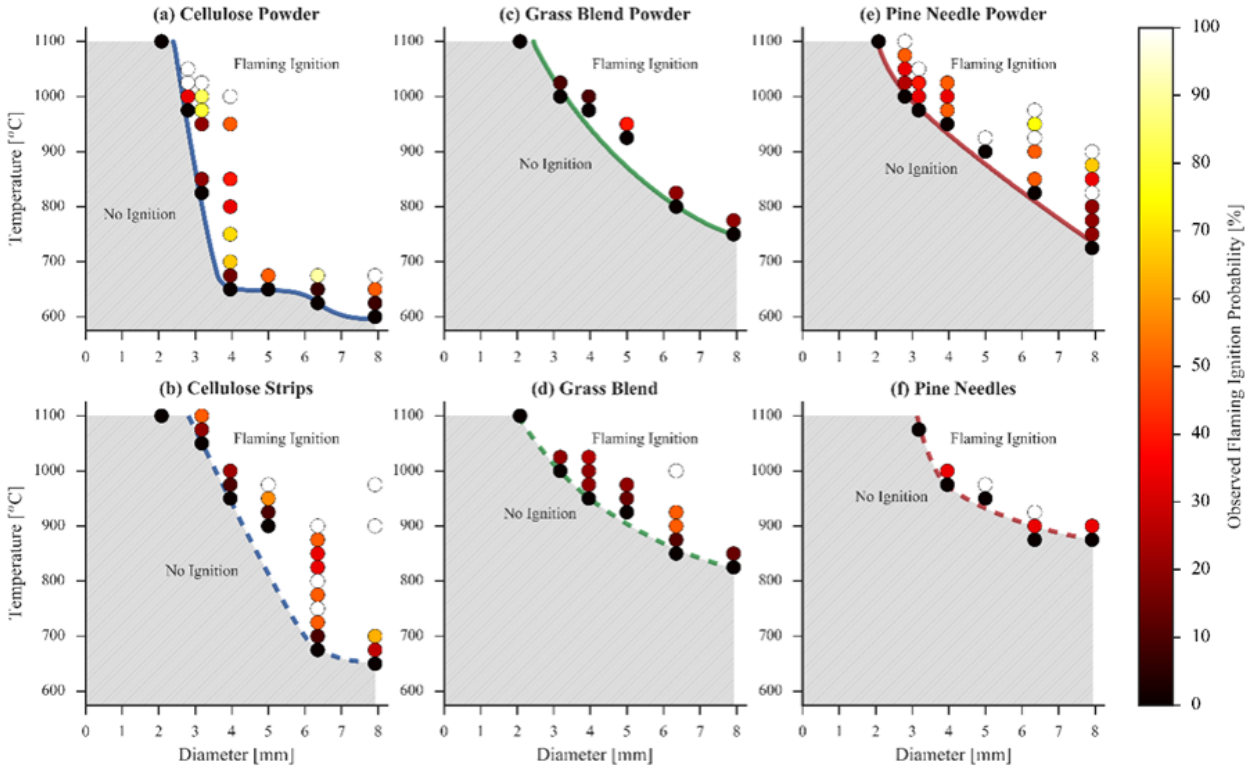

Figure 4.2: Ignition Results for the four fuel beds. Red triangular markers correspond to test conditions where at least one flaming ignition event was observed & black circles correspond to conditions where 10 tests were performed with no flaming ignition events

relatively flat and causes changes in curvature in the curve. This occurs at the melting point of the aluminum alloy, where the melting gives the particles additional energy equivalent to increasing a solid aluminum particle $\sim 400^{o}$C [49, 53, 54].

For direct comparison, the ignition boundaries for the six fuel beds are presented in Fig. 4.3. Also shown in the figure is the flaming ignition boundary for barley grass by contact with hot aluminum particles from Rowntree and Stokes [3]. Looking at the FI boundaries together we can see some trends. The powder fuels (solid lines) are capable of FI at lower particle temperatures than their non-powder counterparts (dashed lines). The pure alpha-cellulose fuels were capable of being ignited by lower temperature particles as compared to the biomass fuels (pine needle fuels and grass blend fuels).

The fact that the powder fuels were capable of ignition at lower temperatures indicates that some combination of smaller fuel particulate sizes and higher densities make ignition possible at lower temperatures. The lower FI boundaries for the alpha-cellulose strips and powder indicate that the components in the biomass fuels other than alpha cellulose such as lignin, hemicellulose, proteins, and ash bearing components make the fuel require higher temperatures for ignition. Thus,

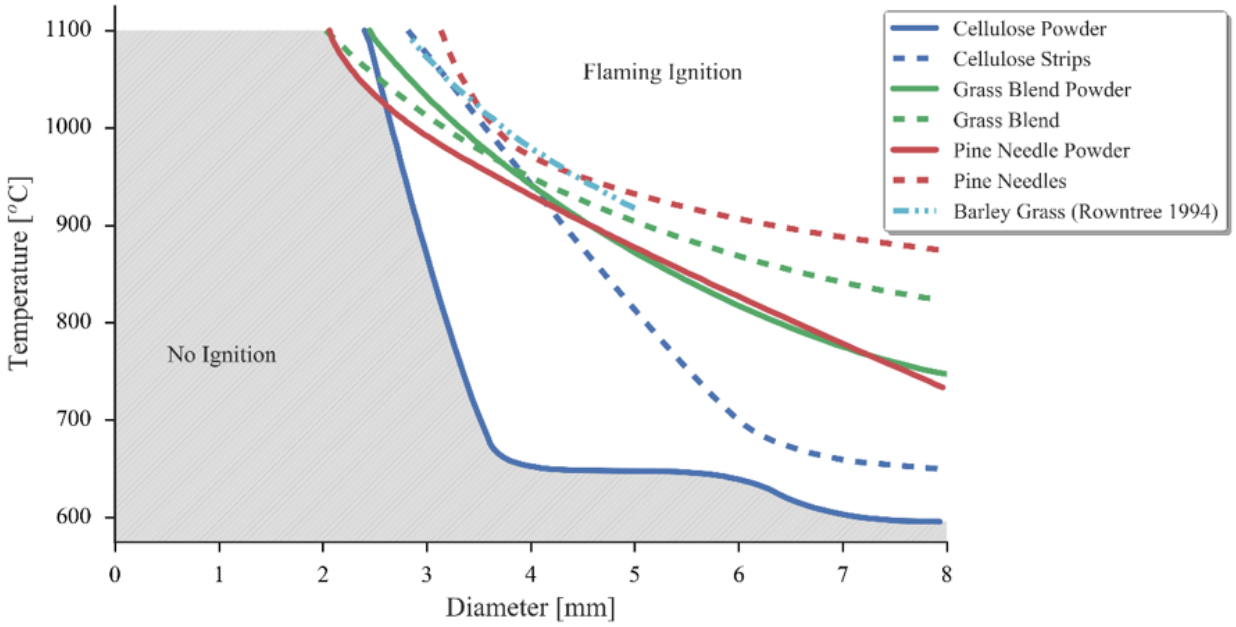

Figure 4.3: Comparison of the ignition boundaries for the six fuel beds. The data from Rowntree and Stokes [3] is also shown for comparison.

both the morphology and chemical composition of the fuel effect the ignition process. Unfortunately, the lack of data at higher temperatures makes it difficult to determine whether there is a minimum particle size required for ignition and if that is dependent the fuel properties studied here. As mentioned earlier, our ability to investigate higher temperature particles was limited by the maximum temperature of the furnace.

The flaming ignition limits for the grass fuels agree well with the flaming ignition results from Rowntree and Stokes[3]. The difference between the ignition boundaries is attributed to different experimental conditions, and a slightly different type of grass as the fuel. The differences in ignition temperatures for the larger particles and the lower temperatures suggests that the ignition process appears to be more of a auto-ignition type. Consequently, the ignition of the fuel by large particles is more sensitive to the type of fuel and its geometry.

simplified Analysis

To examine the effects of the different fuel composition, a simplified analysis of the thermal decomposition reactions (thermal and oxidative pyrolysis) happening in the fuel just before the onset of ignition was developed. Given the short time for ignition to occur ($<$1s) the char oxidation reaction was ignored as it was assumed that minimal char would have accumulated and if it had there would be minimal oxygen available to it. The reaction rates were calculated using the results presented in [4]. The reaction rates were used to calculate an instantaneous heat release rate per

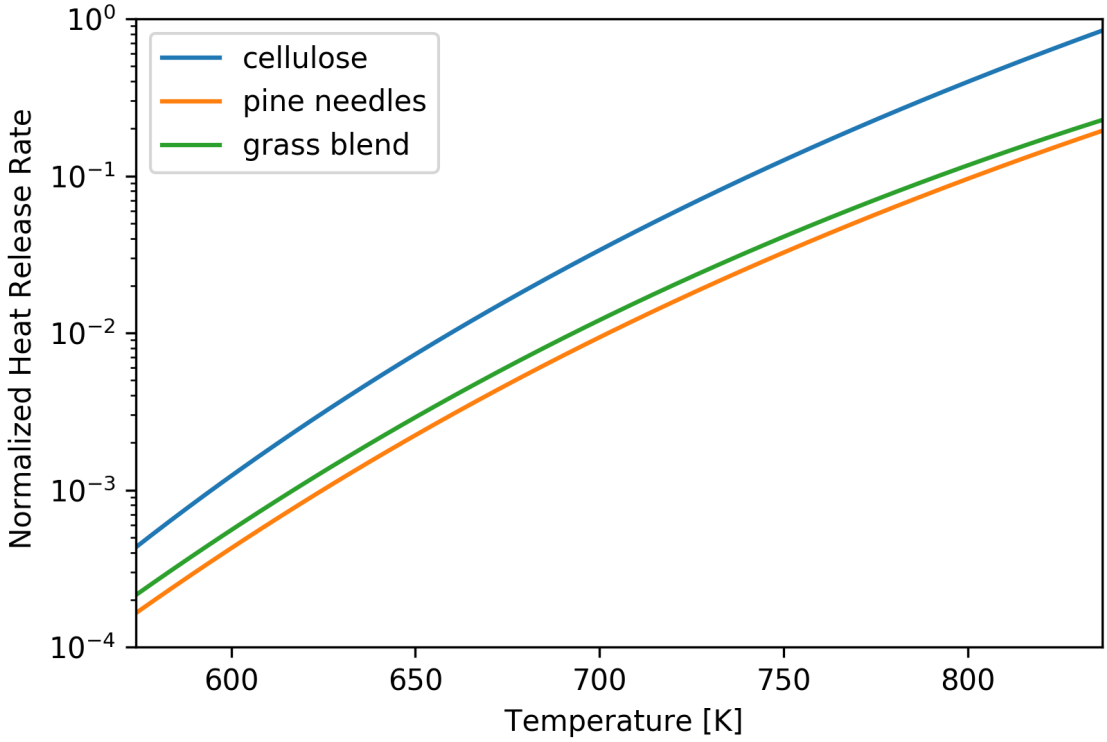

Figure 4.4: Heat released by the solid fuel prior to ignition

unit mass of fuel. The reaction rate of each fuel was calculated by resolving the reaction rates of α cellulose, hemi-cellulose, and lignin and weighting them by their prevalence according to the proximate analysis values taken from the literature which are presented in Table 4.1. The temperatures used were those between the mean of the ambient temperature and the lowest particle temperature (525^{o}C) and the highest particle temperature (1100^{o}C).

The heat release rates are show in Fig. 4.4. The results of this show that all three fuels compositions experienced a net release of heat, with the pure cellulose experiencing the greatest followed by the grass blend, and then closely by the pine needles. These results indicate that the reactions in the solid phase right before ignition in the α-cellulose would be produce more heat which could counteract heat losses from the particle to the fuel, quicken the production of gaseous fuel via the thermal degradation of the solid fuel, and/or potentially raise the temperature of the gaseous products. This could explain the relative ease with which the α-cellulose fuels were ignited compared to the biomass fuels at similar conditions. It should be noted that there are other aspects which could dictate whether or not ignition occurs, namely differences in the chemical composition of the pyrolysis products of the different fuels.

4.3 Conclusions

Experiments were performed investigating the flaming ignition boundaries of alpha-cellulose, a grass blend, and dead pine needles, each tested as powder and with larger fuel particle sizes with lower bulk densities (i.e. paper strips, blades of grass, and pine needles) when they were put in contact with hot aluminum particles. For each fuel bed, the flaming ignition boundaries were determined by finding the lowest particle temperature where flaming ignition occurred. These ignition boundaries separate flaming ignition and non-flaming ignition conditions from each other, and thus which conditions are demonstrably hazardous. The results are consistent with similar studies of hot metal particles igniting fuels where larger particles were capable of igniting fuels at lower temperatures and smaller particles requiring higher temperatures. Thus, the smaller particles require a higher temperature to cause ignition.

It was found that the pure α-cellulose fuels ignite at lower temperatures than the biomass fuels (grass blend and pine needle fuels). This suggests that the additional components found in these fuels such as lignin, hemi-cellulose, other organic compounds as well as the inorganic compounds deter flaming ignition. It was also found that when the fuel is in powder form it is capable of ignition at lower temperature than in strip/grass/needle form confirming that the morphology of the fuel is also important for determining if ignition will occur. However, for the studies presented here the presence of non α-cellulose components had a stronger influence on the ignition process than the fuels morphology.

Chapter 5

Smoldering Spot Ignition of Natural Fuels by a Hot Metal Particle

This work is an experimental and analytical study of how the flaming and smoldering ignition propensities of powdered natural fuel beds in contact with hot metal particles are affected by differences in the particle characteristics, particularly the effect of particle melting, which adds energy to the particle. The smolder data is compared with flaming data including some presented in 4. In the experiments, stainless steel and aluminum particles ranging in size from 1.6 to 8 mm in diameter were heated to various temperatures between 500 and 1100°C and dropped onto a fuel bed composed of a powder grass blend. It is observed that the ignition boundary for smoldering follows a hyperbolic relationship between particle size and temperature similar to results obtained for flaming ignition, with smaller particles requiring higher temperatures to ignite the fuel. For both metal particles smoldering ignition occurs at significantly lower temperatures than flaming ignition. A simplified numerical model is developed to help understand smoldering ignition by a metal particle and to examine how the melting influences the ignition process. Good qualitative agreement is obtained between the model predictions and the experiments suggesting that the model provides a first step toward the theoretical modeling of this complex problem.

This chapter is based on research previously published in *The Proceedings of the Combustion Institute* [50] and presented at *The 2014 Fall Technical Meeting of the Western States Section of the Combustion Institute* [101].

5.1 Experimental Apparatus

The apparatus used for experiments is the same as the one described in 3 with some minor modifications. An overhead camera records images of the tests at regular intervals and captures visible and infrared (IR) light. This allows for visualization of charring of the solid fuel, and heat losses by IR radiation. These pictures provide qualitative data about the temperature of the particle and the presence of solid phase exothermic reactions.

Lab air flows through the wind tunnel with a centerline velocity of .5m/s at the leading edge of

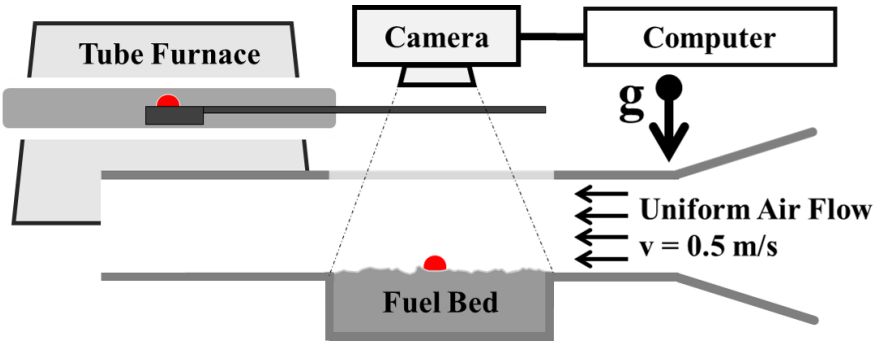

Figure 5.1: Schematic of experimental apparatus

the fuel for all tests. The relative humidity and temperature of the flow were measured daily and found to be on average 31±6% and 24±3°C respectively.

For this study, we used particles composed of stainless steel alloy 302 and 304 [97] and aluminum alloy 1100 [97, 100]. The thermal properties are given in Table 5.1. The particles are spherical or approximately spherical in shape and range in size from 1.6 to 8.0 mm in diameter. The temperatures tested range from 500 to 1100°C. The maximum temperature is limited by the maximum operating temperature of the furnace and no ignition events were observed at the lowest temperature so tests at lower temperatures were not performed. The fuel is a powder formed by grinding a grass blend. The fuel beds were initially bone-dried and then allowed to come to a moisture equilibrium with the air in the laboratory. The fuel moisture content (mass of water to fuel dry mass) of the fuel was measured each day that tests were conducted and the average fuel moisture content for a test was 8.0±2.0%. In order to minimize the effects of random variations in the fuel beds and the fraction of the particle embedded into the fuel, the location where the particle was dropped was varied and no more than two tests of the same condition were done on a single fuel bed.

At least five tests were done at each test condition to determine a probability of ignition. Each test could have one of three outcomes: Flaming Ignition (FI), Smoldering Ignition (SI) or No Ignition (NI). The establishment of self propagating flame spread or large scale smolder spread was not studied here, nor was the possible outcome of a smolder transitioning to a flame. Each of these phenomena are sufficiently complex as to deserve their own study. FI was defined by a flame that persisted for at least 1s. The definition of SI is more difficult because self-sustained smoldering occurs in an opaque medium and is difficult to distinguish from thermal decomposition driven by heat transfer from the particle.

One approach for determining smoldering ignition, used in [102] was to wait for an extended period of time ($> 10^3$s) until the smolder either consumes the entire fuel sample or extinguishes, this was to ensure that a smolder is propagating independently from its ignition source. Due to the large number of tests conducted in this study, we recorded SI when the visible char layer surrounding the particle had a thickness greater that the particle diameter and observed movement

of the smoldering front and pyrolyzate production. This criteria was supported by readings from the IR camera, which showed increasing temperatures after a period of cooling. As a final check, a handful of tests were performed where the smoldering front was allowed to propagate freely through the entire sample over the course of 1hr. A further discussion of the smoldering ignition behavior and associated ignition criteria can be found in Sec. 5.3.

5.2 Model Description

Smoldering ignition of the fuel is simulated with a simplified 1-D spherical model accounting for porous heat and oxygen mass transfer with a 3-step solid phase reaction model. The metal particle was assumed to be thermally lumped and completely surrounded by a virgin material. The outer surface of this virgin material was exposed to air at ambient conditions. The particle is fully submerged in the fuel and only cools by transferring heat to the surrounding material; volatiles that are produced are assumed to instantly leave the domain, oxygen is able to diffuse in from the outer boundary, and the gas phase the density, ρ_g was assumed to be constant. The governing equations of this system are the conservation of energy in the particle, in the solid domain, species conservation in the solid and gas phases in Eqns. 5.2 - 5.4.

$$\left.\frac{\partial T_p}{\partial t}\right|_{r=R_p} = \frac{12\hat{k_s}}{\rho_p c_{p_{eff}(T_p)} R_p}\left.\frac{\partial T_s}{\partial r}\right|_{r=R_p} \tag{5.1}$$

$$\frac{\partial T_s}{\partial t} = \frac{\hat{k_s}}{r^2}\frac{\partial}{\partial r}\left(r^2\frac{\partial T_s}{\partial r}\right) + \sum_j \frac{\Delta H_j \dot{\omega}_j}{\left(\hat{\rho c_p}\right)_s} \tag{5.2}$$

$$\frac{\partial Y_{s,i}}{\partial t} = \sum_j \frac{\nu_{i,j}\dot{\omega}_j}{\hat{\rho}_s} \tag{5.3}$$

$$\frac{\partial Y_{O_2}}{\partial t} = \frac{\hat{\psi} D_{O_2}\rho_g}{r^2}\frac{\partial}{\partial r}\left(r^2\frac{\partial Y_{O_2}}{\partial r}\right) + \sum_j \frac{\nu_{j,O_2}\dot{\omega}_j}{\rho_g \hat{\psi}} \tag{5.4}$$

$$\dot{\omega}_j = Z_j(1-\alpha_j)^{n_j}\left(\frac{Y_{O_2}}{.23}\right)^{n_{O_2,j}} exp\left(\frac{-E_j}{RT_s}\right) \tag{5.5}$$

$$r = R_p \mid T_s = T_{p,o}, \quad \frac{\partial Y}{\partial r}_{O_2} = 0 \tag{5.6}$$

$$r \to \infty \mid T_s = T_\infty, \quad Y_{O_2} = .23\ (Air) \tag{5.7}$$

$$t = 0 \quad \mid T_s = T_\infty,\ Y_{O_2} = .23,\ Y_{virg} = 1 \tag{5.8}$$

where $c_{p,eff}(T_p)$ is an effective specific heat capacity of the particle and k is the effective thermal conductivity which accounts for pore radiation as was done in [54]. For steel, the value for the of the specific heat capacity was constant, while for the aluminum, which melts over the temperature range 643-657°C, the value changes to account for differences in the heat capacity and

Table 5.1: Properties of the fuel species and the particle metals: stainless Steel 302/304 and aluminum 1100. Molten properties shown in parentheses.

Material	Virgin	Char	Ash	Steel	Al. 1100
ρ $[kg/m^3]$	260	90	15	7860	2710 (2375)
c_p $[J/mK]$	1400	1600	1800	500	900 (1141)
k $[W/mK]$	0.1	0.07	0.06	21.5	220 (90.7)
ψ $[-]$	0.35	0.78	0.94	n/a	n/a

Table 5.2: Parameters for Eqn. 5.5: 1) Thermal Pyrolysis and 2) Oxidative pyrolysis and 3) Ashing reactions, values from [4]

j	ΔH $[kJ/kg]$	Z $[1/s]$	E $[kJ/mol]$	n	n_{O_2}
1	0.2	$10^{6.34}$	105	0.87	0
2	-4.3	$10^{8.72}$	128	0.56	0.72
3	-11.9	$10^{6.55}$	124	0.63	0.68

energy added from melting, 390 kJ/kg. D_{O_2} is the mass diffusivity of O_2 in air and taken to be a constant. α_j is the consumption of the j-th solid specie. The initial and boundary conditions are shown in Eqns. 5.6- 5.8.

The solid phase, with exception of the metal particle, was considered to be comprised of three components: Virgin, Char, and Ash with properties show in Table 5.1. The virgin material is the unreacted fuel bed which can react through both thermal and oxidative pyrolysis reactions producing Char. Char can undergo a char oxidation reaction producing Ash, an solid, inert product. This type of 3-step mechanism been applied in other studies of smoldering biomass [4, 103], and the specific thermo-chemical parameters used in this study are given in Table 5.2.

The governing equations were solved with an implicit finite volume scheme with adaptive time stepping. Simulations were performed for particle sizes and temperatures in the same range of those done in the experiments. The minimum initial particle temperature which could ignite a smolder was determined, within 1°C of precision using a root finding algorithm. Smoldering ignition was determined by checking if the smolder would propagate at least 10mm from the particle and show steady or accelerating smolder propagation at this point. The subsequent smolder propagation was not modeled. Simulations were also conducted to observe the events leading up to the initiation of the smoldering front. The computational domain was 37.5mm from the surface of the particle and divided into 10^3 cells for all simulations.

5.3 Results & Discussion

The experimental ignition results are presented in Fig. 5.4. Black circles or squares indicate that no SI or FI events, respectively, were observed and conversely, white circles and squares indicate that all the tests resulted in a SI or FI, respectively. The data is used to find the SI or FI boundaries for the fuel in contact with each type of particle. The ignition boundaries are found by fitting a curve through the data points. Determining precise FI and SI boundaries is difficult as there is a range of test conditions where both SI & NI or FI & SI events were observed. This range is indicative of our ability to control the different parameters of the problem such as the exact fuel porosity at the landing location, variations in the moisture content and ambient conditions. It is possible to use statistical methods to try and determine an average or 50% ignition boundary. In order to do this assumptions must be made regarding the distribution of the variation with respect to each of these parameters/confounding variables and then how precisely they impact the ignition process. In this study we have chosen simply to report ignition boundaries determined by finding a set of maximum temperatures for various particles sizes which did not ignite for at least five tests. We feel that determining the ignition boundaries this way is practical as it reports minimum conditions found to initiate ignition for the study and the criteria for choosing it is simple and well defined.

The primary goal of this study is to identify the required initial particle temperature which would ignite natural fuels with a smolder, but for completeness flaming ignition data is also shown. It is interesting to note that during flaming ignition events, the flame on occasion receded to a smolder after roughly 10s. During each test, the progress of the char front on the surface of the fuel was captured with the overhead camera and two distinct phases of the SI process were observed (see Fig. 5.2). Immediately after landing the particle rapidly heats the surrounding fuel and a *char shell* (typically at least 1mm thick) forms around the particle. This initial smolder will cease to propagate and different sized particles display different behavior. Experiments with small particles will rapidly develop, in roughly 10s, a small localized smolder along the perimeter of the char shell which will may then continue to propagate or extinguish. Experiments with large particles will develop the small localized smolder after a considerably longer time, often as long as 300s, at which point the particle has cooled significantly. The fact that the initial radial smolder stops and then a secondary, self-sustaining smolder, begins later at discreet number of locations (typically only 1 near the ignition limit) around the char shell indicates that there is a process hindering the smolder.

In the first three images of the top and bottom of Fig. 5.2, we see that the particle cools significantly during the course of a test. If a particle cools enough, it could be colder than the temperature of the incipient smolder and heat transfer back to the particle from the smolder might hinder or even prevent the final step of the smoldering ignition. We can examine the effect of heat losses back to the particle through the numerical model. Fig. 5.3, shows the simulated temperature profile of the fuel for a SI case (left) and a NI case (right). The temperature at (x=0) is the temperature of the particle and we can see for the SI case (i) that the particle temperatures initially falls as that energy heats the fuel near the particle. When SI occurs the we see a momentary local maximum in the temperature profile (ii) and then we see the particle temperature rise again (iii) and the reaction front begins to propagate. However, the inherent 1-D aspect of the model does

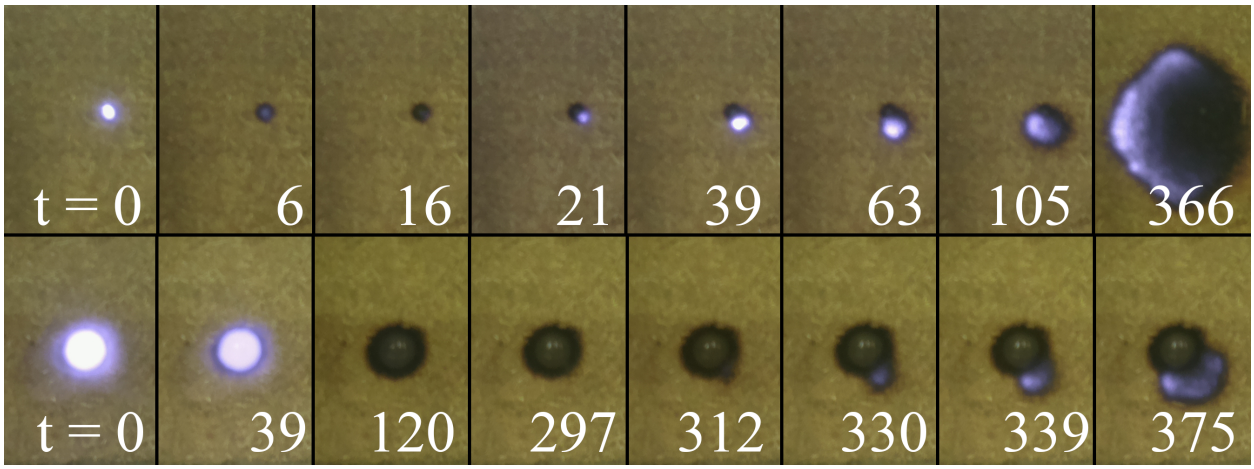

Figure 5.2: Images of surface smolder spread of a 1.6mm steel particle at 1000°C (top) and a 8mm particle initially at 600°C (bottom). The white light is IR light captured by the camera and not visible to the bare eye. Time from impact is shown in seconds for each frame. Note: airflow is coming in from the left. Frames 1-3: Initial cooling for both particles. For the small particle the small localized smolder on the char shell develops 21s after the particle cools in frame 4 and the small localized smolder on the char shell develops at 330s after impact for the large particle in frame 6. Subsequent smolder spread is shown in remaining frames.

not allow it to explain why the secondary self-sustaining smolder starts at only one point from the initial smolder. This is likely caused by small local variations in the fuel bed which cause only one region along the char shell to be viable for the secondary self-sustaining smolder and also by the effects of subsurface smoldering which cannot be visualized by the current model and experimental apparatus. In both the model and the experiments, NI events exhibited the rapid initial radial smolder as with the SI events as shown in the third frame from the left of both the top and bottom of Fig. 5.2 for experiments and the initial spread shown by the model in Fig. 5.3 for the model (iv, v). The smoldering ignition phenomena of the aluminum particles was very similar to those with steel, with exception of the tests where a relatively large aluminum particle was molten. For these experiments there a thicker char shell developed rapid when the particle impacted the fuel, indicating that the energy from melting helps initiate the smolder considerably.

The FI and SI boundaries for each metal type follow the same trend observed in previous work on SI [3, 46] and FI [3, 46, 49] of different fuels. There is a monotonic decrease in the required particle temperature for both SI and FI as the particle size is increased and FI requires higher particle temperatures than SI. We can see that smaller particles had a much larger range of temperatures at which ignition could occur while the range was much smaller for larger particles. At temperatures above 643°C the aluminum alloy used will start to melt, because it is an alloy it melts over a temperature range (643-657°C). We assumed the energy added by melting over this range was linear with respect to temperature. The energy from melting is a likely explanation of

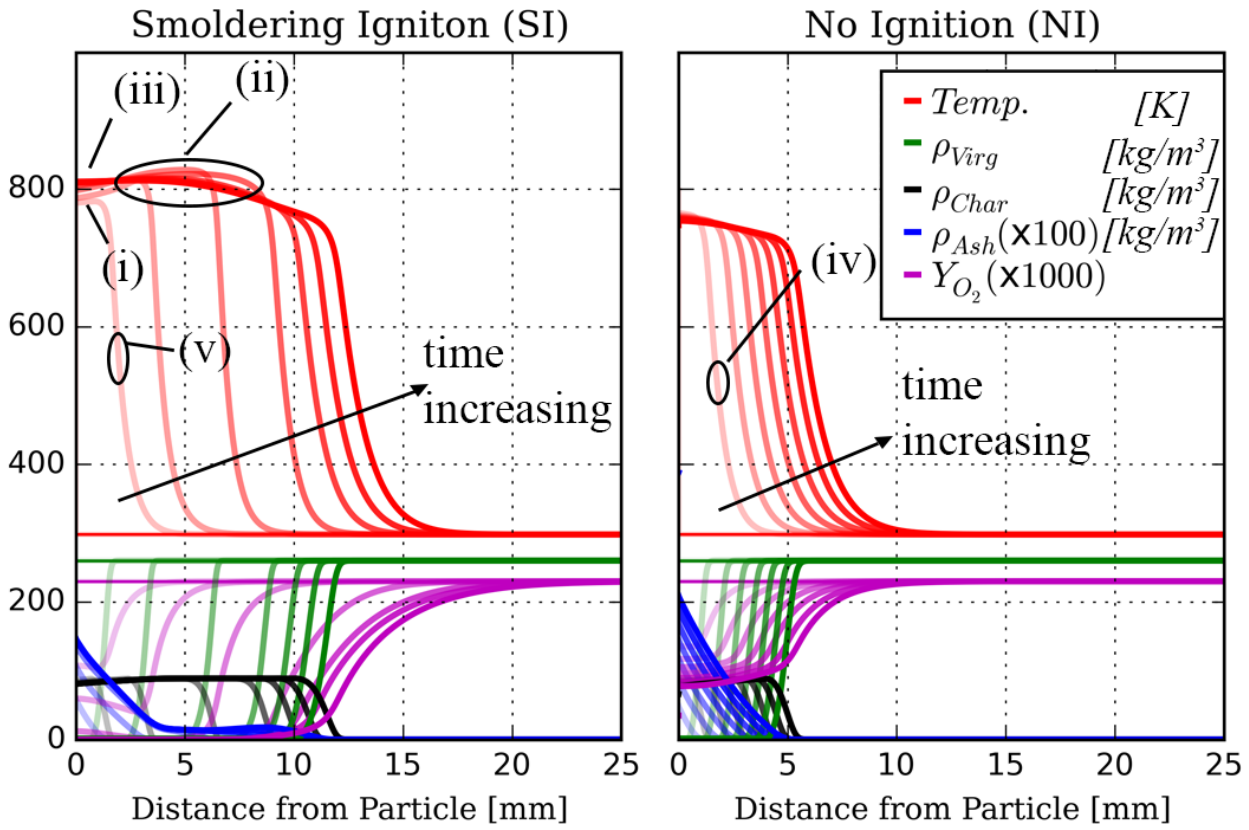

Figure 5.3: Time evolution of 1-D simulations. Both simulations are of 7mm particles. The initial temperature of the particle on the left was 536°C which resulted in SI and the particle on the right was initially at 531°C and resulted in NI. The solution profiles are spaced 10s apart and total time shown in figure is 70s. (i) initial particle cooling due to heat loss to the fuel, (ii) momentary increase in smolder temperature, (iii) particle is heated by the smolder. (iv) & (v) initial smolder/thermal degradation due to heat from the particle

why for particle temperatures greater than or equal to 650°C aluminum particles were able to ignite at lower temperatures than their steel counterparts.

The ignition results from the model show qualitative agreement the experiments. Overall the model predicts ignition at lower temperatures than the experiments. The agreement is within 50°C for particles larger than 4mm. For smaller particles, the model predicts a lower temperatures required for ignition. The likely explanation for this is the cooling of the particle as they fall from the crucible to the fuel. In the case of small particles, higher temperatures are required and the thermal mass of the particle is relatively low so the heat loss rate to the ambient surroundings are more significant than the heat losses for larger, cooler particles. The model presented here is limited as it does not resolve these heat losses. Another limitation of the model that is presented here are the details of the thermal contact between the particle and the surrounding fuel. The

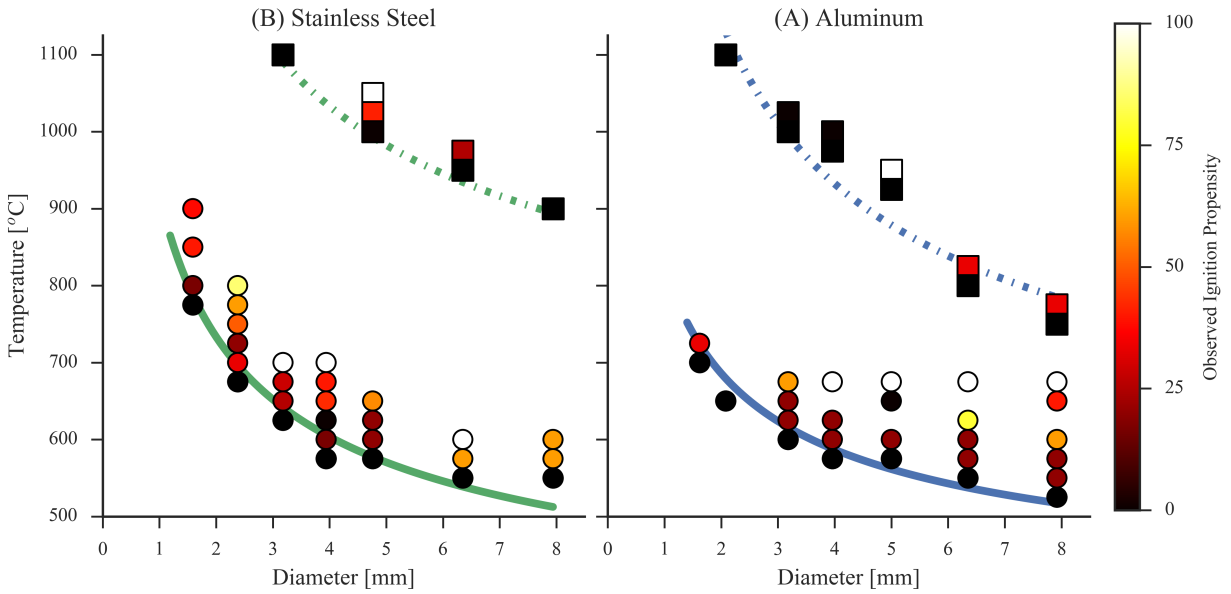

Figure 5.4: Observed Ignition Propensity for (a) Stainless Steel & (b) Aluminum. The squares and circles are colored according to the fraction of the tests that resulted in FI or SI, respectively. Each marker corresponds to at least five tests at that test condition. Ignition boundaries for FI are shown with the dashed lines and for SI with solid lines.

complexities of considering radiative heat transfer from the hot particle and the fuel as studied in [104] were not examined here.

One clear difference in the SI boundaries of the model and experimental data is the effect of melting. The model's SI boundary is nearly a horizontal line for particles smaller than 1mm in size. This behavior was not observed in the experimental SI boundaries. However, the effect of melting can be seen in the upper boundary, showing the minimum temperature where ignition happened during each test. Denoted by the white circles in Fig. 5.4b, we can see that for aluminum particles larger than 3mm in diameter, particles heated to 675°C, the lowest temperature above aluminum's melting range, always ignited while the tests performed 25°C lower had a lower observed ignition probability indicating that the energy added by melting also increases the likelihood of ignition. This effect has also been noticed by the authors for the FI of pure cellulose powder fuels and it was noted that the latent heat of melting adds energy equivalent to the energy gained from heating the aluminum particle an additional 433°C. Thus, a completely molten particle has considerably more energy than a particle just below the melting range, despite the temperature difference of the melting range is only 15°C. This extra energy was also observed to impact the flaming ignition behavior. From Fig. 5.5 it can be seen that the temperatures required for FI are different for the aluminum and stainless steel particles, with the aluminum particles requiring lower temperatures, roughly 100°C lower, for the flaming ignition of the fuel. Despite the difference in temperature,

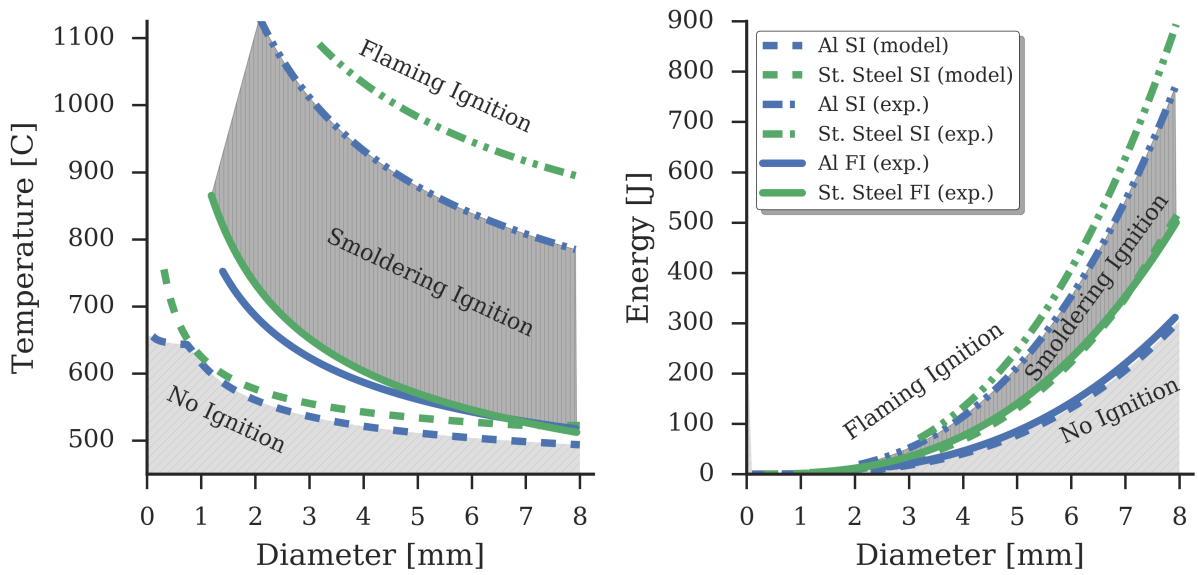

Figure 5.5: Temperature-diameter (a) and Energy-diameter (b) ignition boundaries for Aluminum (blue) and Steel (black) for FI and SI from experiments and SI from the model.

we can see in Fig. 5.5b that the energy of the particles are fairly similar showing that the particle energy is important for ignition.

5.4 Conclusion

Experiments studying flaming and smoldering ignition of a powdered grass blend by contact with hot aluminum and steel particles have been conducted over a wide range of particle sizes and temperatures. The metals used are representative of those which are known to ignite natural fuels in practical settings. They also have different melting temperatures and physical properties. Both metal particles required similar temperatures to initiate a smolder in the fuel. The smoldering ignition behavior of the large particles is sensitive to to the initial particle temperature. For small particles the smoldering ignition behavior was different - aluminum particles were molten and capable of smoldering ignition at lower temperature than their stainless steel counterparts. The process of melting adds extra energy to the molten particles making ignition at lower temperatures possible. Results from the modeling of the smoldering ignition process support the observed importance of initial particle temperature and energy for large and small particles. However from the results of both the model and experiments, ignition cannot be determined simply by the initial particle temperature and energy. The timescales for flaming and smoldering ignition after the particle impacts the fuel are also different. Flaming ignition was observed in the gas phase and

typically occurred on the order of 10-100ms. The initiation of a smoldering independent of the particle took time on the order of 100-1000s and propagated on the surface and inside of the fuel. The results presented here provide a basic understanding of spot fire and spot smolder ignition of biomass/natural fuels by hot metal particles and provide data for verification of theoretical models of this relevant ignition process.

The effects of parameters such as those related to the fuel (chemical composition, moisture content, & morphology), the particle (metal oxidation reactions, & interactions with other particles/accumulation), ambient conditions (air flow, humidity & temperatures) all contribute towards determining the conditions required for FI and SI and thus will affect the ignition boundaries reported here. However, the problem is complex and must be studied in a parametric fashion. There are still aspects of this ignition process that still need to be studied. Many of the parameters, mentioned above, and processes that where not studied here, such as smoldering to flaming transition, should be investigated.

Bibliography

[1] I. Ramljak, ... (ENERGYCON), 2014 IEEE ... (2014) 638–643. URL: http://ieeexplore.ieee.org/xpls/abs_all.jsp?arnumber=6850494.

[2] K. Mikkelsen, An Experimental Investigation of Ignition Propensity of Hot Work Processes in the Nuclear Industry, Ph.D. thesis, University of Waterloo, 2014. URL: https://uwspace.uwaterloo.ca/handle/10012/8396.

[3] G. Rowntree, A. Stokes, Journal of Electrical and Electronics Engineering Australia 14 (1994) 117–123.

[4] A. Anca-Couce, N. Zobel, A. Berger, F. Behrendt, Combustion and Flame 159 (2012) 1708–1719. URL: http://www.sciencedirect.com/science/article/pii/S0010218011003890. doi:10.1016/j.combustflame.2011.11.015.

[5] NFPA, NFPA Standard 51B: Standard for Fire Prevention During Welding, Cutting, and Other Hot Work, Technical Report, National Fire Protection Association, Quincy, MA, 2009.

[6] M. Ahrens, BRUSH , GRASS , AND FOREST FIRES, Technical Report November, NFPA, Quincy, MA, 2013.

[7] N. Z. F. Service, The New Zealand Fire Service Emergency Incident Statistics 2009-2010, Technical Report, New Zealand Fire Service, Wellington, NZ, 2010. URL: http://www.fire.org.nz/about-us/Facts-and-Figures/Documents/Stats-09-10s.pdf.

[8] S. G. Badger, NFPA Journal (2012). URL: http://www.nfpa.org/news-and-research/publications/nfpa-journal/2012/november-december-2012/features/2011-large-loss-fires.

[9] H. Wakelin, Ignition Thresholds for Grassland Fuels and Implications for Activity Controls on Public Conservation Land in Canterbury., Ph.D. thesis, University of Canterbury, 2010. URL: http://www.ir.canterbury.ac.nz/handle/10092/4245.

[10] S. E. Caton, R. S. P. Hakes, D. J. Gorham, A. Zhou, M. J. Gollner, Fire Technology (2016) 1–45. URL: "http://dx.doi.org/10.1007/s10694-016-0601-7. doi:10.1007/s10694-016-0589-z.

[11] J. P. Prestemon, T. J. Hawbaker, M. Bowden, J. Carpenter, M. T. Brooks, K. L. Abt, R. Sutphen, S. Scranton, Wildfire Ignitions: A Review of the Science and Recommendations for Empirical Modeling, Technical Report, US Forest Service, Ashevill, NC, 2013.

[12] J. W. Mitchell, Engineering Failure Analysis 35 (2013) 726–735. doi:10.1016/j.engfailanal.2013.07.006.

[13] M. Gilbert, CalFire Witch Fire Report, Technical Report, California Department of Forestry and Fire Protection (CalFire), Perris, CA, 2008.

[14] W. Mell, Alexander Maranghides, NIST Technical Note 1635: A Case Study of a Community Affected by the Witch and Guejito Fires, Technical Report, 2009. doi:http://iawfonline.org/NIST{_}Witch{_}Fire{_}TN1635.pdf.

[15] D. Heryford, INCIDENT NUMBER : 12-E-CBX COUNTY : Kittitas STATE OF WASHINGTON DEPARTMENT OF NATURAL RESOURCES Southeast Region WILDLAND FIRE INVESTIGATION REPORT, Technical Report, 2012.

[16] J. McGuire, M. Law, J. Miller, Fire Research Notes (1956). URL: http://www.iafss.org/publications/frn/252/-1/view/frn_252.pdf.

[17] J. Arulmoli, B. Vu, M. Sung, Fire and ... (2014) n/a–n/a. URL: http://doi.wiley.com/10.1002/fam.2235http://onlinelibrary.wiley.com/doi/10.1002/fam.2235/full. doi:10.1002/fam.2235.

[18] V. Babrauskas, Ignition Handbook.pd, Fire Science Publishers, Issaquah, WA, 2003.

[19] M. A. Finney, S. S. McAllister, T. B. Maynard, I. J. Grob, Fire Technology (2015). URL: http://link.springer.com/10.1007/s10694-015-0518-6. doi:10.1007/s10694-015-0518-6.

[20] T. Mcdonald, R. Rummer, in: Proceedings of the 33rd Annual meeting of the Council on Forest Engineering: Fueling the Future., pp. 1–12.

[21] J. Song, S. Wang, H. Chen, Theoretical and Applied Mechanics Letters 4 (2014) 034005. URL: http://scitation.aip.org/content/cstam/journal/taml/4/3/10.1063/2.1403405. doi:10.1063/2.1403405.

[22] Y. Hagimoto, K. K, N. Watanabe, K. Okdamoto, in: 6th Indo Pacific Congress on Legal Medicine and Forensic Sciences (INPALMS), Yoyodo, Osaka, pp. 836–866.

[23] K. Kinoshita, Y. Hagimoto, in: Proc. 22nd Annual Meeting Japan Soc. For safety Engrg, pp. 145–148.

[24] M. Shigeta, T. Ikeda, M. Tanaka, T. Suga, B. Poopat, S. Peansukmanee, N. Kunawong, A. Lersvanichkool, H. Kawamoto, S. Thongdee, K. Suenaga, M. Ota, Welding in the World 60 (2016) 355–361. URL: http://download.springer.com/static/pdf/750/art%253A10.1007%252Fs40194-015-0288-2.pdf?originUrl=http%3A%2F%2Flink.springer.com%2Farticle%2F10.1007%2Fs40194-015-0288-2&token2=exp=1496963233~acl=%2Fstatic%2Fpdf%2F750%2Fart%25253A10.1007%25252Fs40194-015-028. doi:10.1007/s40194-015-0288-2.

[25] S. W. Simpson, P. Zhu, Journal of Physics D: Applied Physics 28 (1995) 1594–1600. URL: http://iopscience.iop.org/0022-3727/34/3/317. doi:10.1088/0022-3727/28/8/008.

[26] P. McArdle, A Numerical Model for the Determination of Biomass Ignition from a Hotspot, Ph.D. thesis, 2015. doi:10.1017/CBO9781107415324.004.

[27] A. F. Mills, X. Hang, Fire Technology 20 (1984) 5.

[28] S. L. Manzello, A. Maranghides, W. E. Mell, International Journal of Wildland Fire 16 (2007) 458–462. URL: www.publish.csiro.au/journals/ijwf. doi:10.1071/WF06079.

[29] S. L. Manzello, T. G. Cleary, J. R. Shields, A. Maranghides, W. Mell, J. C. Yang, Fire Safety Journal 43 (2008) 226–233. doi:10.1016/j.firesaf.2006.06.010.

[30] S. L. Manzello, A. Maranghides, J. R. Shields, W. E. Mell, Y. Hayashi, D. Nii, Fire and Materials 33 (2009) 21–31. URL: http://doi.wiley.com/10.1002/fam.977. doi:10.1002/fam.977.

[31] S. L. Manzello, J. R. Shields, T. G. Cleary, A. Maranghides, W. E. Mell, J. C. Yang, Y. Hayashi, D. Nii, T. Kurita, Fire Safety Journal 43 (2008) 258–268. doi:10.1016/j.firesaf.2007.10.001.

[32] S. L. Manzello, T. G. Cleary, J. R. Shields, J. C. Yang, On the ignition of fuel beds by firebrands, Technical Report 1, 2006. URL: http://onlinelibrary.wiley.com/doi/10.1002/fam.901/abstracthttp://doi.wiley.com/10.1002/fam.901. doi:10.1002/fam.901.

[33] S. L. Manzello, T. G. Cleary, J. R. Shields, J. C. Yang, International Journal of Wildland Fire 15 (2006) 427–431. URL: www.publish.csiro.au/journals/ijwf. doi:10.1071/WF06031.

[34] S. L. Manzello, S. H. Park, T. G. Cleary, Fire Safety Journal 44 (2009) 894–900. doi:10.1016/j.firesaf.2009.05.001.

[35] S. L. Manzello, S. Suzuki, Y. Hayashi, in: Fire Safety Journal, volume 54, pp. 181–196. doi:10.1016/j.firesaf.2012.06.012.

[36] A. Tohidi, Experimental and Numerical Modeling of Wildfire Spread via Fire Spotting, Ph.D. thesis, Clemson University, ???? doi:10.13140/RG.2.2.13540.58244.

[37] J. A. Wischkaemper, C. L. Benner, B. D. Russell, Transmission and Distribution Exposition Conference: 2008 IEEE PES Powering Toward the Future, PIMS 2008 (2008) 1–8. doi:10.1109/TDC.2008.4517149.

[38] S. D. Tse, A. Fernandez-Pello, Fire Safety Journal 30 (1998) 333–356. doi:10.1016/S0379-7112(97)00050-7.

[39] I. Glassman, R. A. Yetter, Combustion, Academic Press, 2008.

[40] C. J. Rallis, B. M. Mangaya, Fire Technology 38 (2002) 81–92. doi:10.1023/A:1013484932749.

[41] R. a. Anthenien, S. D. Tse, A. Carlos Fernandez-Pello, Fire Safety Journal 41 (2006) 349–363. URL: http://linkinghub.elsevier.com/retrieve/pii/S0379711206000208. doi:10.1016/j.firesaf.2006.01.005.

[42] F. A. Williams, Combustion Theory, ????

[43] B. Rajmohan, V. Radhakrishnan, Journal of Engineering for Industry 116 (1994) 124. doi:10.1115/1.2901802.

[44] B. Rajmohan, V. Radhakrishnan, International Journal of Machine Tools ... 32 (1992) 563–569. URL: http://ac.els-cdn.com/089069559290045I/1-s2.0-089069559290045I-main.pdf?_tid=e7685cf8-976e-11e4-9439-00000aacb360&acdnat=1420746511_cc885dc02a8d89e7e7f190a477b4cc75http://www.sciencedirect.com/science/article/pii/089069559290045I.

[45] D. G. Howitt, Journal of Fire Sciences 33 (2015) 427–444. URL: http://jfs.sagepub.com/cgi/doi/10.1177/0734904115611820. doi:10.1177/0734904115611820.

[46] R. M. Hadden, S. Scott, C. Lautenberger, a. C. Fernandez-Pello, Fire Technology 47 (2010) 341–355. URL: http://link.springer.com/10.1007/s10694-010-0181-x. doi:10.1007/s10694-010-0181-x.

[47] A. D. Stokes, Journal of Electrical and Electronics Engineering 10 (1990) 188–194.

[48] T. Tanaka, On the Flammability of Combustible Materials By Welding Spatters, Technical Report, Scientific Investigation Research Laboratory, Tottori Police Headquarters, Tottori Prefecture, 1977.

[49] J. L. Urban, C. D. Zak, C. Fernandez-Pello, Proceedings of the Combustion Institute 35 (2014) 2707–2714. URL: http://www.sciencedirect.com/science/article/pii/S1540748914000844. doi:http://dx.doi.org/10.1016/j.proci.2014.05.081.

[50] J. L. Urban, C. D. Zak, J. Song, C. Fernandez-Pello, Proceedings of the Combustion Institute 36 (2016) 3211–3218. URL: http://www.sciencedirect.com/science/article/pii/S1540748916304928http://linkinghub.elsevier.com/retrieve/pii/S1540748916304928www.sciencedirect.com. doi:10.1016/j.proci.2016.09.014.

[51] C. Zak, E. Tjahjono, D. Rich, C. Fernandez-Pello, Forest Fires 2012 (2012).

[52] C. D. Zak, J. L. Urban, C. Fernandez-Pello, Combustion Science and Technology 186 (2014) 1618–1631. URL: http://www.tandfonline.com/doi/abs/10.1080/00102202.2014.935612. doi:10.1080/00102202.2014.935612.

[53] C. Zak, J. L. Urban, V. Tran, C. Fernandez-Pello, in: Fire Safety Science, volume 11, pp. 1368–1378. doi:10.3801/IAFSS.FSS.11-1368.

[54] C. D. Zak, The Effect of Particle Properties on Hot Particle Spot Fire Ignition, Ph.D. thesis, University Of California Berkeley, 2015.

[55] S. Wang, X. Huang, H. Chen, N. Liu, International Journal of Wildland Fire 26 (2017) 71–81. doi:10.1071/WF16096.

[56] a. C. Fernandez-Pello, C. Lautenberger, D. Rich, C. Zak, J. L. Urban, R. Hadden, S. Scott, S. Fereres, Combustion Science and Technology 187 (2014) 269–295. URL: http://www.tandfonline.com/doi/abs/10.1080/00102202.2014.973953. doi:10.1080/00102202.2014.973953.

[57] J. L. Urban, C. Zak, A. Fernandez-Pello, Fire Technology (2017) (submitted).

[58] S. Wang, H. Chen, L. Zhang, Journal of Applied Polymer Science 131 (2014) n/a–n/a. URL: http://doi.wiley.com/10.1002/app.39359. doi:10.1002/app.39359.

[59] S. Wang, X. Huang, H. Chen, N. Liu, G. Rein, Combustion and Flame 162 (2015) 4112–4118. URL: http://linkinghub.elsevier.com/retrieve/pii/S0010218015002849http://www.sciencedirect.com/science/article/pii/S0010218015002849. doi:10.1016/j.combustflame.2015.08.017.

[60] G. Wang, Who will pay the bill for the massive CCTV fire ?, 2015. URL: http://news.xinhuanet.com/english/2009?02/18/content_10842463.htm.

[61] T. H. Huang, S. T. Thynell, K. Kuo, Journal of Propulsion and Power 11 (1995) 781–790. URL: http://arc.aiaa.orghttp://dx.doi.org/10.2514/3.23903. doi:10.2514/3.23903.

[62] P. Yin, N. Liu, H. Chen, J. S. Lozano, Y. Shan, Fire Technology 50 (2014) 79–91. doi:10.1007/s10694-012-0272-y.

[63] K. McGratten, S. Hostikka, J. Floyd, H. Baum, R. Rehm, NIST Special Publication 1018-5 Fire Dynamics Simulator Technical Reference Guide, Technical Report, NIST, ???? URL: http://www.vtt.fi/inf/julkaisut/muut/2007/NIST_SP_1018_5.pdf.

[64] C. Lautenberger, Fire Safety Science 11 (2014) 193–207. URL: http://www.iafss.org/publications/fss/11/193. doi:10.3801/IAFSS.FSS.11-193.

[65] C. Lautenberger, A. C. Fernandez-Pello (????).

[66] C. Lautenberger, A. C. Fernandez-Pello, in: WIT Transactions on Modelling and Simulation, volume 48, WIT Press, 2009, pp. 603–612. URL: http://library.witpress.com/viewpaper.asp?pcode=CMEM09-054-1. doi:10.2495/CMEM090541.

[67] S. L. Manzello, Y. Hayashi, T. Yoneki, Y. Yamamoto, Fire Safety Journal 45 (2010) 35–43. doi:10.1016/j.firesaf.2009.09.002.

[68] S. L. Manzello, S. Suzuki, D. Nii, Fire Technology 53 (2017) 535–551. URL: http://link.springer.com/10.1007/s10694-015-0537-3. doi:10.1007/s10694-015-0537-3.

[69] H. Abuluwefa, R. I. L. Guthrie, F. Ajerscht, Oxidation of Metals 46 (1996) 423–440. doi:10.1007/BF01048639.

[70] R. Y. Chen, W. Y. D. Yuen, Oxidation of Metals 59 (2003) 433–468. doi:10.1023/A:1023685905159.

[71] J.-H. Sun, R. Dobashi, T. Hirano, Combustion Science and Technology 150 (2000) 99–114. URL: http://www.tandfonline.com/doi/pdf/10.1080/00102200008952119. doi:10.1080/00102200008952119.

[72] E. L. Dreizin, Progress in Energy and Combustion Science 26 (2000) 57–78. URL: http://www.sciencedirect.com/science/article/pii/S0360128599000106. doi:10.1016/S0360-1285(99)00010-6.

[73] H. R. Lawless, K. R. Lawless, Rep. Prog. Phys 37 (1974) 231–316. URL: http://stacks.iop.org/0034-4885/37/i=2/a=002?key=crossref.92a0c85c090f91f58ed375a548082571http://iopscience.iop.org/0034-4885/37/2/002. doi:10.1149/1.3071795.

[74] W. Tomlinson, P. Lidgitt, Corrosion Science 12 (1972) 807–810. doi:10.1016/S0010-938X(72)90304-6.

[75] A. G. Goursat, W. W. Smeltzert, Oxidation of Metals 6 (1973) 101–116.

[76] X. Chunhua, G. Wei, Mat Res innovat 3 (2000) 231–235. doi:10.1007/s100190050008.

[77] R. E. Carter, The Journal of Chemical Physics 34 (1961) 2010. URL: http://scitation.aip.org/content/aip/journal/jcp/34/6/10.1063/1.1731812. doi:10.1063/1.1731812.

[78] G. Garnaud, R. a. Rapp, Oxidation of Metals 11 (1977) 193–198. doi:10.1007/BF00606543.

[79] F. Gesmundo, F. Viani, Corrosion Science 18 (1978) 231–243. URL: http://www.sciencedirect.com/science/article/pii/S0010938X78800195. doi:10.1016/S0010-938X(78)80019-5.

[80] H. S. Hsu, Oxidation of Metals 26 (1986) 315–332. doi:10.1007/BF00659339.

[81] Z. Xu, X. Sun, M. A. Khaleel, The Journal of Chemical Physics 074702 (2012). URL: http://dx.doi.org/10.1063/1.4740242http://aip.scitation.org/toc/jcp/137/7. doi:10.1063/1.4740242.

[82] P. N. Daykin, Journal of the Fisheries Research Board of Canada 22 (1965) 159–171. doi:10.1139/f65-014.

[83] W. Mallard, P. Linstrom (Eds.), NIST Chemistry webBook, NIST Standard Reference Database Number 69, Gaithersburg MD, 20899, 2014. URL: http://webbook.nist.gov/chemistry. doi:citeulike-article-id:3211271.

[84] J. L. Urban, C. D. Zak, C. Fernandez-Pello, in: 2014 Western States Section of the Combustion Institute (WSSCI) Spring Meeting, Pasadena, CA.

[85] J. C. Thomas, R. M. Hadden, A. Simeoni, Experimental investigation of the impact of oxygen flux on the burning dynamics of forest fuel beds, 2017. URL: http://ac.els-cdn.com/S0379711217301790/1-s2.0-S0379711217301790-main.pdf?_tid=81f9be54-6d93-11e7-8f9e-00000aacb361&acdnat=1500586776_6947f1e7dd2cf3746a6488998fd548d8. doi:10.1016/j.firesaf.2017.03.086.

[86] R. S. Silver, The London, Edinburgh, and Dublin Philosophical Magazine and Journal of Science 23 (1937).

[87] D. Rich, C. Lautenberger, J. L. Torero, J. G. Quintiere, C. Fernandez-Pello, Proceedings of the Combustion Institute 31 (2007) 2653–2660. URL: http://linkinghub.elsevier.com/retrieve/pii/S154074890600318X. doi:10.1016/j.proci.2006.08.055.

[88] J. L. Urban, C. Zak, C. Fernandez-Pello, in: AOFST10, Tskuba, Japan.

[89] J. L. Urban, C. D. Zak, C. Fernandez-pello, in: Fire and Materials Conference.

[90] ASTM-E11-17, ASTM Standard Guide E11-17 (2013) 9. URL: https://compass.astm.org/Standards/HISTORICAL/E11-13.htm. doi:10.1520/E0011-13.2.

[91] Alfalfa King, Welcome to Oat , Wheat & Barley Hay, 2014. URL: http://www.alfalfaking.com/oat-wheat-barley/.

[92] I.W. Tremont, Cellulose Paper, 2014. URL: http://www.iwtremont.com/products/specialtyProducts.php.

[93] Sigma Aldrich, Alpha Cellulose Specifications Sheet, ???? URL: http://www.sigmaaldrich.com/Graphics/COfAInfo/SigmaSAPQM/SPEC/C8/C8002/C8002-BULK_____SIGMA_____.pdf.

[94] M. .-B. Johansson, Forestry 68 (1995) 49–62. URL: http://forestry.oxfordjournals.org/cgi/doi/10.1093/forestry/68.1.49. doi:10.1093/forestry/68.1.49.

[95] P. McKendry, Bioresource Technol 83 (2002) 37–46. URL: http://www.sciencedirect.com/science/article/pii/S0960852401001183http://dx.doi.org/10.1016/S0960-8524(01)00118-3. doi:10.1016/S0960-8524(01)00118-3.

[96] S. Mani, L. G. Tabil, S. Sokhansanj, Biomass and Bioenergy 30 (2006) 648–654. URL: http://linkinghub.elsevier.com/retrieve/pii/S0961953406000250. doi:10.1016/j.biombioe.2005.01.004.

[97] Matweb, 1100 Aluminum, 2015. URL: http://www.matweb.com/search/datasheet.aspx?MatGUID=ff6d4e6d529e4b3d97c77d6538b29693.

[98] M. J. Assael, K. Kakosimos, M. R. Banish, J. Brillo, I. Egry, R. Brooks, P. N. Quested, K. C. Mills, A. Nagashima, Y. Sato, W. A. Wakeham, J. Phys. Chem. Ref. Data 35 (2006). URL: http://dx.doi.org/10.1063/1.2149380. doi:10.1063/1.2149380.

[99] E. H. Buyco, F. E. Davis, J. Chem. Eng. Data 15 (1970). doi:10.1021/je60047a035.

[100] C. Y. Ho, R. W. Powell, P. E. Liley, Journal of Physical and Chemical Reference Data 1 (1972) 279. URL: http://scitation.aip.org/content/aip/journal/jpcrd/1/2/10.1063/1.3253100. doi:10.1063/1.3253100.

[101] J. L. Urban, C. D. Zak, J. Song, C. Fernandez-Pello, in: 2016 Fall Technical Meeting of the Western States Section of the Combustion Institute, Seattle, WA.

[102] R. Anthenien, A. Fernandez-Pello, The 27th Symposium (International) on Combustion 27 (1998) 2683–2690. doi:10.1016/S0082-0784(98)80124-0.

[103] T. Ohlemiller, Progress in Energy and Combustion Science 11 (1985) 277–310. URL: http://www.sciencedirect.com/science/article/pii/0360128585900048. doi:10.1016/0360-1285(85)90004-8.

[104] J. Yang, S. Wang, H. Chen, International Journal of Heat and Mass Transfer 97 (2016) 146–156. URL: http://www.sciencedirect.com/science/article/pii/S0017931015304014. doi:10.1016/j.ijheatmasstransfer.2016.01.070.